Also available from Routledge

Atmosphere, Weather and Climate, fifth edition
Roger G. Barry and Richard J. Chorley

Mountain, Weather and Climate, second edition
Roger G. Barry

Climate since AD 1500
R. Bradley and P. Jones

Climate Data and Resources: A Reference and Guide
Edward Linacre

Global Environmental Issues, second edition
David D. Kemp

Climate, History and the Modern World
H.H. Lamb

Climate: Past, Present and Future
H.H. Lamb

The Big Smoke
Peter Brimblecombe

T. R. OKE

BOUNDARY LAYER CLIMATES

Second edition

Routledge
Taylor & Francis Group
LONDON AND NEW YORK

Symbols

Symbol	*Quantity*	*SI Units*
Roman capital letters		
A	horizontal moisture transport in the air per unit horizontal area	$kg\,m^{-2}\,s^{-1}$
	area	m^2
A'	lot area	m^2
A^*	silhouette area	m^2
B	water intake by an animal	kg, $kg\,m^{-2}\,s^{-1}$
C	heat capacity of a substance	$J\,m^{-3}\,K^{-1}$
D	diffuse short-wave radiation	$W\,m^{-2}$
	Dalton Number (Appendix A2)	
E	evapotranspiration	mm, $kg\,m^{-2}\,s^{-1}$
ELR	environmental lapse rate	$K\,m^{-1}$
F	anthropogenic water release due to combustion (Chapter 8)	mm, $kg\,m^{-2}\,s^{-1}$
F_C	carbon dioxide flux density	$kg\,m^{-2}\,s^{-1}$
F_P	pollution flux density	$kg\,m^{-2}\,s^{-1}$
H	height	m
H_s	effective stack height (Chapter 9)	m
I	piped water supply per unit horizontal area (Chapter 8)	mm, $kg\,m^{-2}\,s^{-1}$
	radiant intensity (Appendix A1)	$W\,sr^{-1}$
I_0	solar constant	$W\,m^{-2}$
J	vertical flux of soil water	$kg\,m^{-2}\,s^{-1}$
K^*	net short-wave radiation	$W\,m^{-2}$
$K\downarrow$	incoming short-wave radiation	$W\,m^{-2}$
$K\uparrow$	reflected short-wave radiation	$W\,m^{-2}$
K_f	hydraulic conductivity	$mm\,d^{-1}$
K_C	eddy diffusion coefficient for CO_2	$m^2\,s^{-1}$

Symbol	*Quantity*	*SI Units*
K_{Ex}	extraterrestrial solar radiation	$W m^{-2}$
K_H	eddy conductivity	$m^2 s^{-1}$
K_M	eddy viscosity	$m^2 s^{-1}$
K_P	eddy diffusion coefficient for pollution	$m^2 s^{-1}$
K_V	eddy diffusivity for water vapour	$m^2 s^{-1}$
L	latent heat, of fusion (L_f), of vaporization (L_v), of sublimation (L_s)	$J kg^{-1}$
L^*	net long-wave radiation	$W m^{-2}$
$L\downarrow$	incoming long-wave radiation from the atmosphere	$W m^{-2}$
$L\uparrow$	outgoing long-wave radiation from a surface	$W m^{-2}$
M	flux density of water melt or freeze	mm, $kg m^{-2} s^{-1}$
N	diffuse irradiance	$W m^{-2} sr^{-1}$
P	total atmospheric pressure	Pa
	rate of gross photosynthesis (Chapter 4)	$kg m^{-2} s^{-1}$
	wave period (Chapter 2)	s
	population of a settlement (Chapter 8)	
Q	heat energy	J
Q^*	net all-wave radiation flux density	$W m^{-2}$
$Q\downarrow$	total incoming short- and long-wave radiation	$W m^{-2}$
$Q\uparrow$	total outgoing short- and long-wave radiation	$W m^{-2}$
Q_A	horizontal energy transport in the air per unit horizontal area	$W m^{-2}$
Q_E	turbulent latent heat flux density	$W m^{-2}$
Q_F	anthropogenic heat flux density due to combustion	$W m^{-2}$
Q_G	sub-surface heat flux density	$W m^{-2}$
Q_H	turbulent sensible heat flux density	$W m^{-2}$
Q_M	metabolic heat production by animals (Chapter 6)	$W m^{-2}$
Q_P	rate of energy storage in photosynthesis	$W m^{-2}$
Q_R	rate of heat supply by rainfall	$W m^{-2}$
R	rate of CO_2 respiration by plants	$kg m^{-2} s^{-1}$
Ri	Richardson's Number	
S	direct-beam short-wave radiation	$W m^{-2}$
	soil moisture content or water storage	
T	temperature	K, (°C)
T_b	animal body (or core) temperature	K, (°C)
U	urinary water loss by an animal	kg, $kg m^{-2} s^{-1}$
V	voltage	V
W	width	m
X	length	m
Z	solar zenith angle	

Symbol	*Quantity*	*SI Units*
	Roman small letters	
a	extinction coefficient	m^{-1}
c	specific heat of a substance	$J kg^{-1} K^{-1}$
c_p	specific heat of air at constant pressure	$J kg^{-1} K^{-1}$
d	zero plane displacement	m
e	vapour pressure; saturation value (e*)	Pa
	base of Naperian logarithms	
f	moisture infiltration	mm, $kg m^2 s^{-1}$
g	acceleration due to gravity	$m s^{-2}$
h	height of an object (e.g. crop or shelterbelt)	m
	hour angle	
h^*	depth of the surface mixed layer	m
h_s	stack height	m
k	thermal conductivity	$W m^{-1} K^{-1}$
	von Karman's constant	m
m	optical air mass number	
p	precipitation	mm
r	resistance to flow	$s m^{-1}$
	radius	
r_a	aerodynamic resistance	$s m^{-1}$
r_b	laminar boundary layer resistance	$s m^{-1}$
r_c	canopy (or surface) resistance	$s m^{-1}$
r_m	mesophyll resistance	$s m^{-1}$
r_{st}	stomatal resistance	$s m^{-1}$
s	slope of the saturation vapour versus temperature curve	$Pa K^{-1}$, $kg m^{-3} K^{-1}$
t	time	s
u	horizontal wind speed	$m s^{-1}$
	optical depth of water vapour	mm
u_*	friction velocity	$m s^{-1}$
vdd	vapour density deficit	$kg m^{-3}$
vpd	vapour pressure deficit	Pa
w	vertical wind speed	$m s^{-1}$
x	horizontal (along-wind) distance	m
y	horizontal (across-wind) distance	m
z	vertical distance	m
z_0	roughness length	m

Symbol	*Quantity*	*SI Units*
	Greek capital letters	
Γ	dry adiabatic lapse rate	$K\,m^{-1}$
Δ	finite difference approximation (i.e. difference or net change in a quantity)	
ΔA	net moisture advection; rate per unit volume (per unit horizontal area)	kg; $kg\,m^{-3}\,s^{-1}$ ($kg\,m^{-2}\,s^{-1}$)
ΔP	net rate of photosynthesis, rate of net CO_2 assimilation	$kg\,m^{-2}\,s^{-1}$
ΔQ_A	net energy (sensible and latent) advection; rate per unit volume (per unit horizontal area)	J; $W\,m^{-3}$ ($W\,m^{-2}$)
ΔQ_M	net latent heat storage change due to melting/freezing; rate per unit volume (per unit horizontal area)	J; $W\,m^{-3}$ ($W\,m^{-2}$)
ΔQ_P	net energy storage due to photosynthesis; rate per unit volume (per unit horizontal area)	J; $W\,m^{-3}$ ($W\,m^{-2}$)
ΔQ_S	net energy storage; rate per unit volume (per unit horizontal area)	J; $W\,m^{-3}$ ($W\,m^{-2}$)
ΔS	net moisture storage; rate per unit volume (per unit horizontal area)	kg; $kg\,m^{-3}\,s^{-1}$; ($kg\,m^{-2}\,s^{-1}$)
Δh	height of plume rise	m
Δr	net run off	mm, $kg\,m^{-2}\,s^{-1}$
Θ	zenith angle	
Φ_C, Φ_H, Φ_M, Φ_V	dimensionless stability functions for carbon dioxide, heat, momentum and water vapour respectively.	
X	rate of pollution emission	$kg\,m^{-2}\,s^{-1}$, $m^3\,s^{-1}$
Ψ	soil moisture potential	Pa
	transmissivity	
Ω	solar azimuth angle	
	Greek small letters	
α	surface albedo	
β	Bowen's ratio (Q_H/Q_E)	
	elevation angle	

Symbol	*Quantity*	*SI Units*
γ	psychrometric constant	$Pa\,K^{-1}$; $kg\,m^{-3}\,K^{-1}$
γ^*	apparent psychrometric constant	$Pa\,K^{-1}$; $kg\,m^{-3}\,K^{-1}$
δ	solar declination angle	
ε	surface emissivity	
ζ	absorptivity	
θ	potential temperature	K
κ	thermal diffusivity of a substance	$m^2\,s^{-1}$
κ_H, κ_M, κ_V	molecular diffusion coefficients for heat, momentum (viscosity) and water vapour in air	$m^2\,s^{-1}$
λ	wavelength	m
μ	thermal admittance	$J\,m^{-2}\,s^{-1/2}\,K^{-1}$
ρ	density of a substance: of air ρ_a; of CO_2 ρ_c; of water vapour ρ_v; water ρ_w	$kg\,m^{-3}$
ρ_v^*	saturation water vapour density	$kg\,m^{-3}$
σ	Stefan-Boltzmann constant	$W\,m^{-2}\,K^{-4}$
σ_y, σ_z	standard deviations of horizontal and vertical pollutant distribution	m
τ	momentum flux per unit surface area	Pa
ϕ	heat of assimilation of carbon	$J\,kg^{-1}$
	latitude	
χ	concentration of an air pollutant	$kg\,m^{-3}$, ppm
ψ	view factor	
ω	solid angle	sr

Common subscripts

(A)	Atmosphere
(E)	Earth
a	air
(b)	bottom (abaxial) surface of a leaf
c	cloud
	canopy
f	forest floor; fusion
h	horizontal
i	normal incidence
l	liquid
long	long-wave
max	maximum
min	minimum

Symbol Quantity

o	surface
(o)	cloudless
r	rural
s	soil; sublimation
short	short-wave
sky	sky
(t)	top (adaxial) surface of a leaf
u	urban
v	vapour
λ	wavelength

Superscripts

∧	sloping surface
—	time average
′	instantaneous deviation from mean
~	spatial average

Part I
Atmospheric systems

1 Energy and mass exchanges

1 ATMOSPHERIC SCALES

The Atmosphere is characterized by phenomena whose space and time scales cover a very wide range. The space scales of these features are determined by their typical size or wavelength, and the time scales by their typical lifetime or period. Figure 1.1 is an attempt to place various atmospheric phenomena (mainly associated with motion) within a grid of their probable space and time limits. The features range from small-scale turbulence (tiny swirling eddies with very short life spans) in the lower left-hand corner, all the way up to jet streams (giant waves of wind encircling the whole Earth) in the upper right-hand corner.

In reality none of these phenomena is discrete but part of a continuum, therefore it is not surprising that attempts to divide atmospheric phenomena into distinct classes have resulted in disagreement with regard to the scale limits. Most classification schemes use the characteristic horizontal distance scale as the sole criterion. A reasonable consensus of these schemes gives the following scales and their limits (see the top of Figure 1.1):

Micro-scale	10^{-2} to 10^{3} m
Local scale	10^{2} to 5×10^{4} m
Meso-scale	10^{4} to 2×10^{5} m
Macro-scale	10^{5} to 10^{8} m

In these terms this book is mainly restricted to atmospheric features whose horizontal extent falls within the micro- and local scale categories. A fuller description of its scope is given by also including characteristic vertical distance, and time scales.

This book is concerned with the interaction between the Atmosphere and the Earth's surface. The influence of the surface is effectively limited to the lowest 10 km of the Atmosphere in a layer called the *troposphere*

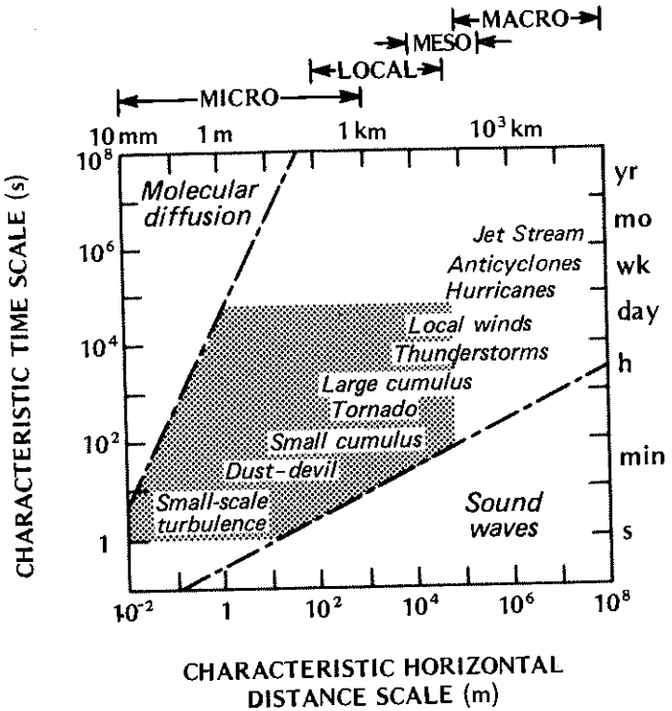

Figure 1.1 Time and space scales of various atmospheric phenomena. The shaded area represents the characteristic domain of boundary layer features (modified after Smagorinsky, 1974).

(Figure 1.2). (*Note* – terms introduced for the first time are italicized and the meaning of those not fully explained in the text is given in Appendix A5.) Over time periods of about one day this influence is restricted to a very much shallower zone known as the *planetary or atmospheric boundary layer*, hereinafter referred to simply as the *boundary layer*. This layer is particularly characterized by well developed mixing (turbulence) generated by frictional drag as the Atmosphere moves across the rough and rigid surface of the Earth, and by the 'bubbling-up' of air parcels from the heated surface. The boundary layer receives much of its heat and all of its water through this process of turbulence.

The height of the boundary layer (i.e. the depth of surface-related influence) is not constant with time, it depends upon the strength of the surface-generated mixing. By day, when the Earth's surface is heated by the Sun, there is an upward transfer of heat into the cooler Atmosphere. This vigorous thermal mixing (convection) enables the boundary layer depth to extend to about 1 to 2 km. Conversely by night, when the Earth's

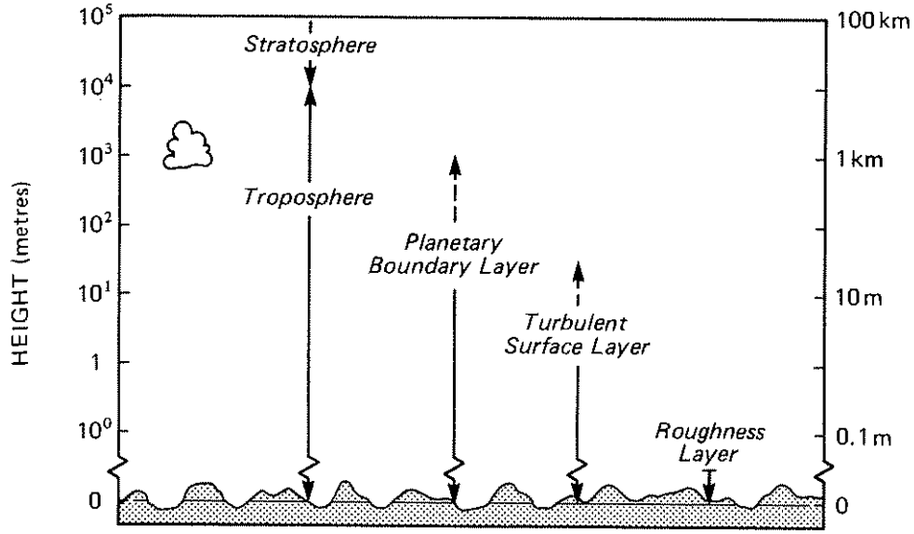

Figure 1.2 The vertical structure of the atmosphere.

surface cools more rapidly than the Atmosphere, there is a downward transfer of heat. This tends to suppress mixing and the boundary layer depth may shrink to less than 100 m. Thus in the simple case we envisage a layer of influence which waxes and wanes in a rhythmic fashion in response to the daily solar cycle.

Naturally this ideal picture can be considerably disrupted by large-scale weather systems whose wind and cloud patterns are not tied to surface features, or to the daily heating cycle. For our purposes the characteristic horizontal distance scale for the boundary layer can be related to the distance air can travel during a heating or cooling portion of the daily cycle. Since significant thermal differences only develop if the wind speed is light (say less than 5 m s^{-1}) this places an upper horizontal scale limit of about 50 to 100 km. With strong winds mixing is so effective that small-scale surface differences are obliterated. Then, except for the dynamic interaction between airflow and the terrain, the boundary layer characteristics are dominated by tropospheric controls. In summary the upper scale limits of boundary layer phenomena (and the subject matter of this book) are vertical and horizontal distances of ~1 km and ~50 km respectively, and a time period of ~1 day.

The *turbulent surface layer* (Figure 1.2) is characterized by intense small-scale turbulence generated by the surface roughness and convection; by day it may extend to a height of about 50 m, but at night when the boundary layer shrinks it may be only a few metres in depth. Despite its variability in the short term (e.g. seconds) the surface layer is horizontally

homogeneous when viewed over longer periods (greater than 10 min). Beneath the surface layer are two others that are controlled by surface features, and whose depths are dependent upon the dimensions of the surface roughness elements. The first is the *roughness layer* which extends above the tops of the elements to at least 1 to 3 times their height or spacing. In this zone the flow is highly irregular being strongly affected by the nature of the individual roughness features (e.g. blades of grass, trees, buildings, etc.). The second is the *laminar boundary layer* which is in direct contact with the surface(s). It is the non-turbulent layer, at most a few millimetres thick, that adheres to all surfaces and establishes a buffer between the surface and the more freely diffusive environment above. The dimensions of the laminar boundary layer define the lower vertical size scale for this book.

The lower horizontal scale limit is dictated by the dimensions of relevant surface units and since the smallest climates covered are those of insects and leaves, this limit is of the order of 10^{-2} to 10^{-3} m. It is difficult to set an objective lower cut-off for the time scale. An arbitrary period of approximately 1 s is suggested.

The shaded area in Figure 1.1 gives some notion of the space and time bounds to boundary layer climates as discussed in this book (except that it requires a third co-ordinate to show the vertical space scale). Two aberrations from this format should be noted. First, it should be pointed out that precipitation and violent weather events (such as tornadoes), which might be classed as boundary layer phenomena, have been omitted. The former, although deriving their initial impetus near the surface, owe their internal dynamics to condensation which often occurs at the top or above the boundary layer. The latter are dominated by weather dynamics occurring at much larger scales than outlined above. Second, the boundary layer treated herein includes the uppermost layer of the underlying material (soil, water, snow, etc.) extending to a depth where diurnal exchanges of water and heat become negligible.

2 A SYSTEMS VIEW OF ENERGY AND MASS EXCHANGES AND BALANCES

The classical climatology practised in the first half of the twentieth century was almost entirely concerned with the distribution of the principal climatological parameters (e.g. air temperature and humidity) in time and space. While this information conveys a useful impression of the state of the atmosphere at a location it does little to explain how this came about. Such parameters are really only indirect measures of more fundamental quantities. Air temperature and humidity are really a gauge of the thermal energy and water status of the atmosphere respectively, and these are tied to the fundamental energy and water cycles of the *Earth-Atmosphere*

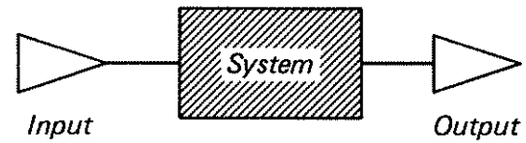

Figure 1.3 Energy flow through a system.

system. Study of these cycles, involving the processes by which energy and mass are transferred, converted and stored, forms the basis of modern physical climatology.

The relationship between energy flow and the climate can be illustrated in the following simple manner. The First Law of Thermodynamics (conservation of energy) states that energy can be neither created nor destroyed, only converted from one form to another. This means that for a simple system such as that in Figure 1.3, two possibilities exist. Firstly:

$$\text{Energy Input} = \text{Energy Ouptut} \tag{1.1}$$

in this case there is no change in the net energy status of the system through which the energy has passed. It should however be realized that this does not mean that the system has no energy, merely that *no change* has taken place. Neither does it mean that the Output energy is necessarily in the same *form* as it was when it entered. Energy of importance to climatology exists in the Earth-Atmosphere system in four different forms (*radiant*, *thermal*, *kinetic* and *potential*) and is continually being transformed from one to another. Hence, for example, the Input energy might be entirely radiant but the Output might be a mixture of all four forms. Equally the Input and Output *modes* of energy transport may be very different. The exchange of energy within the Earth-Atmosphere system is possible in three modes (*conduction*, *convection* and *radiation* (see Section 3 for explanation)).

The second possibility in Figure 1.3 is:

$$\text{Energy Input} = \text{Energy Output} + \text{Energy Storage Change}$$

For most natural systems the equality, Input = Output, is only valid if values are integrated over a long period of time (e.g. a year). Over shorter periods the energy balance of the system differs significantly from equality. The difference is accounted for by energy accumulation or depletion in the system's energy store. (The energy storage term may have a positive or negative sign. By convention a positive storage indicates the addition of energy.) In climatic terms, for example, if energy is being accumulated in a soil-atmosphere system it probably means an increase in soil and/or air temperature.

Hence we see the link between process (energy flow) and response (temperature change). The whole relationship is referred to as a *process-response system*, which in essence describes the connection between cause

and effect. The degree of detailed understanding of the system depends on how well the internal workings of the 'box' in Figure 1.3 are known. Inside the box the energy is likely to be channelled into different subsystems, and converted into different combinations of energy forms and modes of transport. Some will lead to energy storage change and others to energy output from the system. This partitioning is not haphazard, it is a function of the system's physical properties. In the case of energy these properties include its ability to absorb, transmit, reflect and emit radiation, its ability to conduct and convect heat, and its capacity to store energy.

In the analogous case of water flow in a soil-atmosphere system the mass of water is conserved at all times but it may be found in three different *states* (vapour, liquid and solid); be transported in a number of modes (including convection, precipitation, percolation, and runoff); and its accumulation or depletion in stores is measured as changes of water content (atmospheric humidity, soil moisture or the water equivalent of a snow or ice mass). Similar analogues can be extended to the mass balances of other substances cycled through systems as a result of natural or human (anthropogenic) activities including sulphur, carbon, nitrogen, and particulates. In the case of atmospheric systems the accumulation of these substances beyond certain levels constitutes atmospheric pollution. This occurs when the natural cycling of substances is upset by human activities. For example, in urban areas, if the emission (input) of these materials exceeds the physical capability of the local atmospheric system to flush itself (output) in a short period of time, the result is an increase in the local concentration of that substance (i.e. increased storage). Therefore in the most general form we may write the following energy or mass balance equation for a system:

$$\text{Input} - \text{Output} - \text{Storage Change} = 0 \qquad (1.2)$$

There are two fundamental cycles of importance in understanding atmospheric systems. These are the cycles of solar energy (heat), and water (mass). The remainder of this chapter is concerned with a description of the workings of these two cycles. This is followed in Chapter 2 by an explanation of the way these exchange processes and balances are linked to the vertical distributions of such climatological elements as temperature, humidity and wind speed in the boundary layer.

3 ENERGY BALANCES

(a) Radiation characteristics

Radiation is a form of energy due to the rapid oscillations of electromagnetic fields. It is transferred by *photons*, or bundles of energy that have properties similar to both particles and waves. The oscillations may be

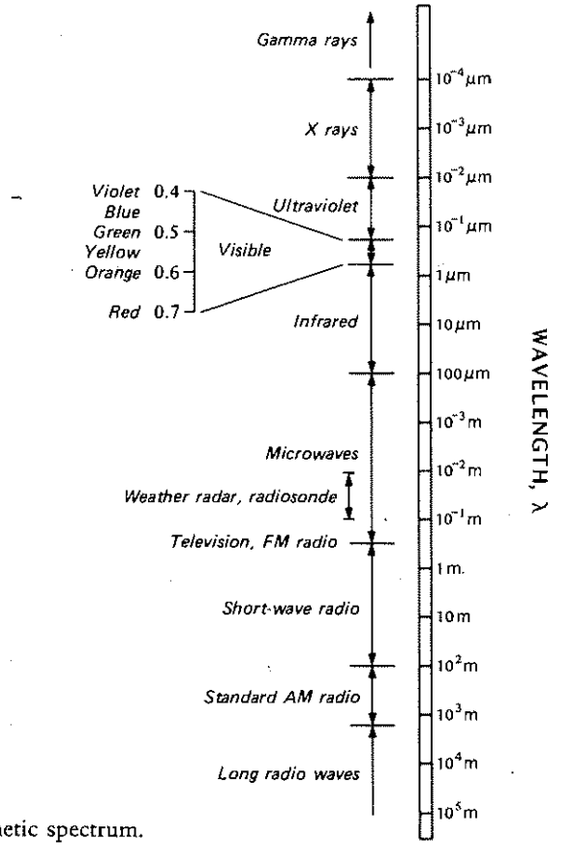

Figure 1.4 The electromagnetic spectrum.

considered as travelling waves characterized by their wavelength λ (distance between successive wavecrests). In most atmospheric applications we are concerned with wavelengths in the approximate range 0·1 to 100 μm (1 μm = 10^{-6} m), representing only a very small portion of the total electromagnetic spectrum (Figure 1.4). The visible portion of the spectrum, to which the human eye is sensitive, is an even smaller fraction extending from 0·36 μm (violet) to 0·75 μm (red). Radiation is able to travel in a vacuum, and all radiation moves at the speed of light (3×10^8 m s^{-1}), and in a straight path. The wavelength is uniquely related to the photon energy so that it is possible to calculate the photon energy flux at any given wavelength or waveband (see Appendix A4f, p. 399).

All bodies possessing energy (i.e. whose temperatures are above absolute zero, 0 K = − 273·2°C, see p. 395) emit radiation. If a body at a given temperature emits the maximum possible amount of radiation per unit of its surface area in unit time then it is called a *black body* or *full radiator*. Such a body has a surface *emissivity* (ε) equal to unity.

Less efficient radiators have emissivities between zero and unity. The relation between the amount of radiation emitted by a black body, and the wavelength of that radiation at a given temperature is given by Planck's Law. In graphical form this law shows the spectral distribution of radiation from a full radiator to be a characteristic curve (Figure 1.5). The shape consists of a single peak of emission at one wavelength (λ_{max}), and a tailing-off at increasingly higher wavelengths. The form is so characteristic that in Figure 1.5 the same Planck curve on different scales, describes the emission spectra from full radiators at 300 and 6000 K. However, the total amount of radiation given out and its spectral composition are very different for the two cases.

The total energy emitted by each body in Figure 1.5 is proportional to the area under the curve (including the tail at longer wavelengths that has been truncated). This is the basis of the Stefan–Boltzmann Law:

$$\text{Energy emitted} = \sigma T_0^4 \tag{1.3}$$

where, σ – Stefan–Boltzmann proportionality constant = $5{\cdot}67 \times 10^{-8}$ W m^{-2} K^{-4}, and T_0 – surface temperature of the body (K). In the typical range of temperatures encountered in the E-A system (−15 to 45°C) a change of 1 K in T_0 of a full radiator results in a change of the emitted radiation of between 4 and 7 W m^{-2} (see Appendix A3, p. 394). If the body is not a full radiator, equation 1.3 can be re-written to include the value of the surface emissivity:

$$\text{Energy emitted} = \varepsilon\sigma T_0^4. \tag{1.4}$$

Note that the energy emission given by these equations is the *radiant flux* (rate of flow of radiation) (J s^{-1} = W) from unit area (m^2) of a plane surface into the overlying hemisphere. The flux per unit area of a quantity is termed its *flux density* (W m^{-2}). Further, *irradiance* is the radiant flux density incident on a surface whereas *emittance* is the radiant flux density emitted by a surface.

The effect of temperature change on the wavelength composition of the emitted radiation is embodied in Wien's Displacement Law. It states that a rise in the temperature of a body not only increases the total radiant output, but also increases the proportion of shorter wavelengths of which it is composed. Thus as the temperature of a full radiator increases, the Planck curve is progressively shifted to the left, and the wavelength of peak emission (λ_{max}) moves with it so that:

$$\lambda_{max} = 2{\cdot}88 \times 10^{-3}/T_0 \tag{1.5}$$

with λ_{max} in metres and T_0 on the Kelvin scale.

The temperatures in Figure 1.5 were chosen because they approximately represent the average surface temperatures of the Sun and the E-A system,

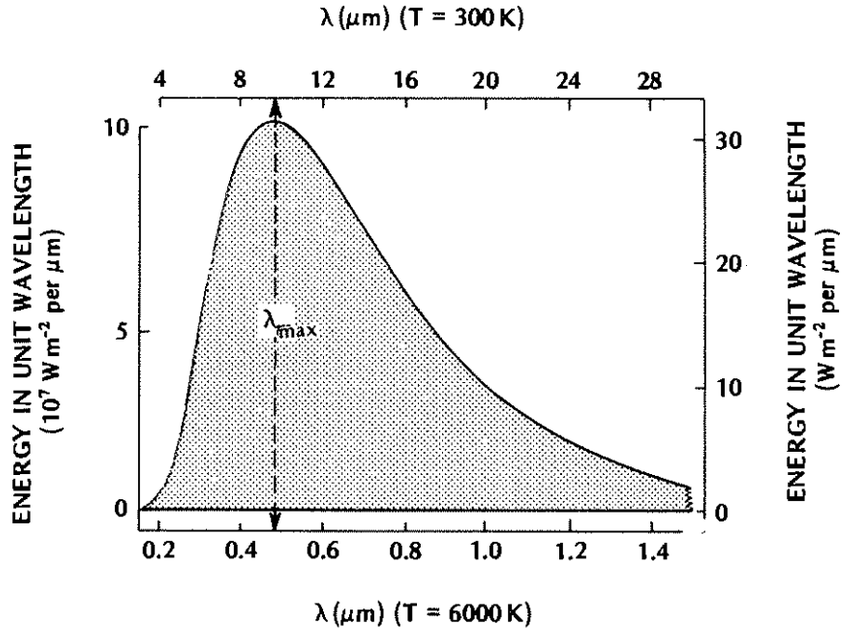

Figure 1.5 Spectral distribution of radiant energy from a full radiator at a temperature of (a) 6000 K, left-hand vertical and lower horizontal axis, and (b) 300 K, right-hand vertical and upper horizontal axis. λ_{max} is the wavelength at which energy output per unit wavelength is maximal (after Monteith, 1973).

and thus illustrate the nature of the radiation each emits. Obviously the E-A system emits smaller total amounts of energy than the Sun, but also the wavelength composition is very different. From equation 1.5 it can be seen that the Sun's peak wavelength is about 0·48 μm (in the middle of the visible spectrum), whereas for the E-A system it is about 10 μm. Typical wavelengths for radiation from the Sun extend from 0·15 μm (ultra-violet) to about 3·0 μm (near infra-red), whereas E-A system radiant wavelengths extend from 3·0 μm to about 100 μm, well into the infra-red. In fact the difference between the two radiation regimes is conveniently distinct; about 99% of the total energy emitted by the two planets lies within these limits. On this basis atmospheric scientists have designated the radiation observed in the range 0·15–3·0 μm to be *short-wave* or *solar radiation*, and that in the range 3·0–100 μm to be *long-wave* radiation.

Radiation of wavelength λ incident upon a substance must either be transmitted through it or be reflected from its surface, or be absorbed. This is a statement of the conservation of energy. By expressing the proportions transmitted, reflected and absorbed as ratios of the incident energy, we

Table 1.1 Radiative properties of natural materials.

Surface	Remarks	Albedo α	Emissivity ε
Soils	Dark, wet	0·05–0·40	0·98–0·90
	Light, dry		
Desert		0·20–0·45	0·84–0·91
Grass	Long (1·0 m)	0·16–0·26	0·90–0·95
	Short (0·02 m)		
Agricultural crops, tundra		0·18–0·25	0·90–0·99
Orchards		0·15–0·20	
Forests			
Deciduous	Bare	0·15–0·20	0·97–0·98
	Leaved		
Coniferous		0·05–0·15	0·97–0·99
Water	Small zenith angle	0·03–0·10	0·92–0·97
	Large zenith angle	0·10–1·00	0·92–0·97
Snow	Old	0·40–0·95	0·82–0·99
	Fresh		
Ice	Sea	0·30–0·45	0·92–0·97
	Glacier	0·20–0·40	

Sources: Sellers (1965), List (1966), Paterson (1969) and Monteith (1973).

define the transmissivity (Ψ_λ), the reflectivity (α_λ) and the absorptivity (ζ_λ) and it follows that:

$$\Psi_\lambda + \alpha_\lambda + \zeta_\lambda = 1 \tag{1.6}$$

These are radiative properties of the substance (expressed as dimensionless numbers between zero and unity). Strictly equation 1.6 is only valid for the case of a single wavelength. In practice it is usually acceptable for fairly wide wavebands (e.g. for solar radiation α is referred to as the surface *albedo* – see Table 1.1 for typical values). It is however essential that each property refers to the same incident radiation.

It can also be shown that for the same radiation:

$$\zeta_\lambda = \varepsilon_\lambda \tag{1.7}$$

This is Kirchhoff's Law, which holds that at the same temperature and wavelength good absorbers are good emitters. It follows that for a full radiator $\zeta_\lambda = \varepsilon_\lambda = 1$, and from equation (1.6) $\alpha_\lambda = \Psi_\lambda = 0$. Further, for

an opaque ($\Psi_\lambda = 0$) non-black body there is some reflection which is given by:

$$\alpha_\lambda = 1 - \zeta_\lambda = 1 - \varepsilon_\lambda \tag{1.8}$$

In boundary layer climatology these relations are very helpful in long-wave exchange considerations (i.e. between bodies at typical E-A system temperatures). Although they are theoretically valid for short-wave exchange, their use does not arise because no E-A system bodies emit short wavelength radiation. Typical values of long-wave surface emissivity (ε) for natural surfaces are given in Table 1.1. It is readily apparent that most of these surfaces are close to being full radiators (ε typically greater than 0·90), so that reflection of long-wave radiation is small (i.e. from equation 1.8 α_{long} is generally less than 0·10).

During its passage through the Atmosphere the solar beam encounters clouds and other atmospheric constituents including water vapour, salt crystals, dust particles and various gases. Each of these constituents has its own set of radiative properties with respect to the incident short-wave radiation, thus part of the beam is reflected (scattered), a part is absorbed and the rest is transmitted to the surface. The ratio of the extraterrestrial input to these amounts defines the atmospheric reflectivity, absorptivity and transmissivity (α_a, ζ_a and Ψ_a).

The nature and amount of absorption depends on the absorption spectra of the atmospheric gases (Figure 1.6) and of cloud and other aerosols. Figure 1.6 demonstrates that the Atmosphere is not a very good absorber of short-wave radiation (0·15–3·0 μm). Ozone (O_3) is very effective at filtering out ultra-violet radiation at wavelengths less than 0·3 μm, and water vapour becomes increasingly important at greater than 0·8 μm, but in the intervening band where the intensity of solar radiation is greatest (i.e. near $\lambda_{\max}$ in Figure 1.5) the Atmosphere is relatively transparent. Even the absorption by liquid water drops in cloud is relatively small.

The portion of the incoming solar radiation that is reflected and scattered, together with that multiply-reflected between the surface and the atmosphere (back-scattered), gives *diffuse* short-wave radiation (D). As an approximation we may consider this radiant receipt to arrive from all parts of the sky hemisphere, although in cloudless conditions it is greater from the area of the sky around the solar disc and near the horizon. Clouds are very effective at diffusing short-wave radiation.

Finally, the portion of the incoming solar radiation that arrives at the Earth's surface, without being absorbed or diffused, is called the *direct-beam* short-wave radiation (S). Since it can be approximated as a parallel beam, the irradiance of an exposed surface depends on its orientation to the beam such that:

$$S = S_i \cos\Theta \tag{1.9}$$

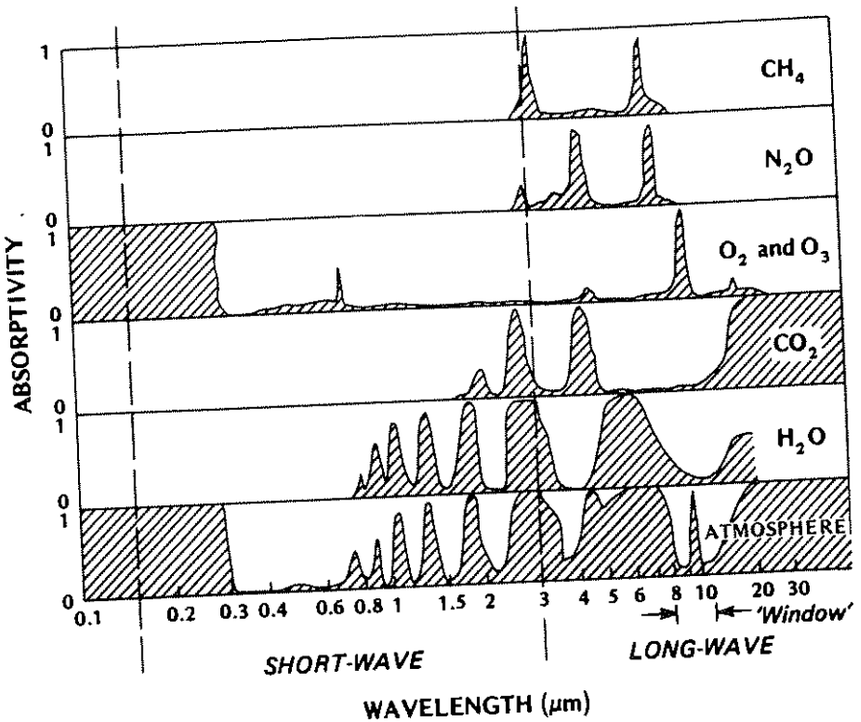

Figure 1.6 Absorption at various wavelengths by constituents of the Atmosphere, and by the Atmosphere as a whole (after Fleagle and Businger, 1963).

where S is the flux density of the beam radiation at the surface, S_i is the flux density normal to the beam and Θ is the angle between the beam and the normal to the surface. This corollary of Lambert's Law (Appendix A1, p. 350), called the *cosine law of illumination*, is illustrated in Figure 1.7a, which shows that the greater the angle to the surface the larger is the area over which it is spread and hence the less the irradiance. (*Note* – in order to generalize equation 1.9 it is necessary to know the surface geometry and the azimuth and zenith angles of the Sun, see Appendix A1.)

The total short-wave radiation received at the surface ($K\downarrow$) is simply:

$$K\downarrow = S + D \tag{1.10}$$

as illustrated in Figure 1.7b.

The process of long-wave radiative exchange in the Atmosphere is very complex. At all levels the Atmosphere absorbs long-wave radiation arriving from below (emitted from the surface and lower layers of air and cloud) and from above (higher layers of air and cloud). The absorption depends upon the long-wave absorptivities of the constituents present. In

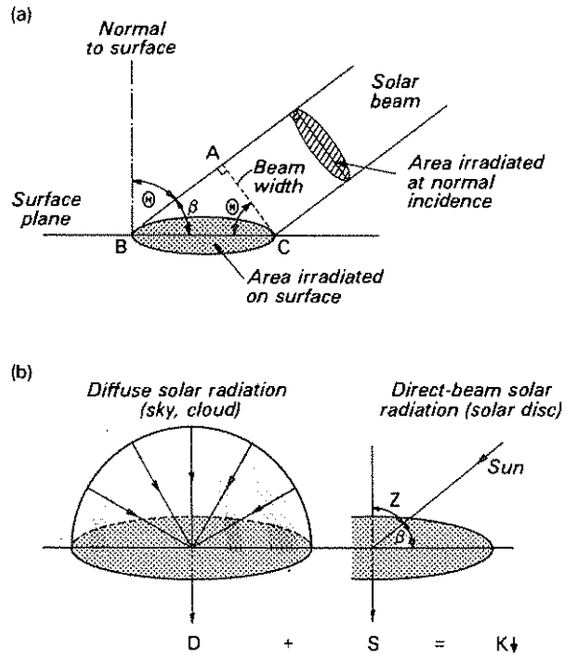

Figure 1.7 (a) Illustration of the areas irradiated by a circular beam on planes placed normal to, and at an angle Θ to, the beam. The radiant energy flux (J s^{-1}) is spread over unit area ($= \pi(0{\cdot}5AC)^2$) at normal incidence but over a larger area ($= \pi(0{\cdot}5BC)^2$) on the surface. The flux density (W m^{-2}) on the surface (S) is less than that at normal incidence (S_i) by the ratio AC/BC = $\cos\Theta$ or $\sin\beta$. Therefore, $S = S_i \cos\Theta$ and when $\Theta = 0°$ $\cos\Theta = 1$ and $S = S_i$. For a horizontal surface $\Theta = Z$ the zenith angle of the Sun. (b) The components of incoming solar radiation at the Earth's surface (modified after Monteith, 1973).

general the Atmosphere is a relatively good absorber in the long-wave band (3 to 100 μm). As shown in Figure 1.6, this is particularly due to the absorptivities of water vapour (H_2O), carbon dioxide (CO_2) and ozone (O_3). Of these, water vapour is by far the most important. If liquid water is present, as cloud droplets, the absorptivity is even greater. There is, however, one important gap in a cloudless Atmosphere's absorption spectrum for long-wave radiation. Except for a narrow band of ozone absorption (9·6 to 9·8 μm), the Atmosphere is open to the transmission of radiation in the 8 to 11 m band. This gap is called the *atmospheric*

'window'. It is through this 'window' that most of the E-A system long-wave loss to Space occurs. However, even this 'window' can be partially closed by clouds or atmospheric pollutants.

At all levels the atmosphere emits long-wave radiation consistent with its temperature (T_a) and emissivity (ε_a) in accord with equation 1.4. We might also note that from Kirchhoff's Law since $\zeta_\lambda = \varepsilon_\lambda$, just as the Atmosphere does not absorb in the 'window' region, it also will not emit those wavelengths. The atmospheric emission is directed both upwards and downwards. The processes of absorption and re-emission take place on a continuous basis throughout the Atmosphere, but quantitatively they are most important in the lowest layers where the concentrations of water vapour and carbon dioxide are greatest. The net portion which emerges from the top of the Atmosphere is lost to Space, and that which arrives at the Earth's surface is sometimes referred to as *counter-radiation* ($L\downarrow$) because it counteracts the outgoing long-wave radiation from the surface ($L\uparrow$). As with the diffuse solar radiation it is usually acceptable to assume that $L\downarrow$ arrives equally from all parts of the sky hemisphere. In reality it is greatest from areas near the horizon and least from the zenith (directly overhead the point of concern).

Conduction

Thermal *conduction* is the process whereby heat is transmitted within a substance by the collision of rapidly moving molecules. It is usually an effective mode of transfer in solids, less so in liquids and least important in gases. In general pure molecular conduction is negligible in atmospheric applications, except within the very thin laminar boundary layer (p. 37). On the other hand it is very important to the transport of heat beneath the surface. The conduction of heat is dependent on the thermal properties of the substrate. Theoretical considerations are covered in Chapter 2.

Convection

The process of *convection* involves the vertical interchange of air masses and can only occur in liquids and gases. In the Atmosphere the parcels of air (or *eddies*) transport energy and mass from one location to another. The eddies may be set into turbulent motion by free or forced convection. *Free convection* is due to the parcel of air being at a different density than the surrounding fluid. If for example a parcel is warmer than its surroundings, it will be at a lower density and will tend to rise. Conversely, if it is cooler it will be denser and tend to sink. The motion of water in a heated kettle is free convection, and a similar 'bubbling-up' of air parcels occurs when the Earth's surface is strongly heated by solar radiation. If the state of the Atmosphere is conducive to free convection it is said to be *unstable*,

and if it inhibits such motion it is *stable* (see p. 51). The atmosphere near the Earth's surface may also be physically thrown into motion when it flows over obstacles. This is *forced*, or *mechanical*, *convection* and depends upon the roughness of the surface and the speed of the horizontal flow. Often free and forced convection co-exist giving *mixed convection*.

If the addition or subtraction of energy to a body is sensed as a rise or fall in its temperature then it is referred to as *sensible heat*. On the other hand, to enable a substance to change from liquid at a given temperature to vapour *at the same temperature*, requires the addition of heat. This heat which is not sensed as a temperature change is called *latent heat*. It is locked up within the substance and is available for release should the substance revert to its former state. Energy is taken up to move in the direction of a higher energy state (e.g. solid to liquid, or liquid to vapour) and released in moving in the opposite direction.

Convection transports heat to and from the Atmosphere in both its sensible and latent forms. Sensible heat is carried from a warmer surface into the cooler air above by turbulent eddies and is released when it mixes with the environmental air. The reverse transport occurs when the air is warmer than the surface. Latent heat transport is tied up with that of water vapour. The latent heat imparted to a parcel of moist air in the evaporation of water at the surface is liberated to warm the air when the water vapour condenses into cloud. Convection provides the means of transport and mixing.

This process is also responsible for the exchanges of carbon dioxide and pollutants between the surface and the Atmosphere and also for the extraction of momentum from the mean flow. The essential principles governing convective (turbulent) transport in the boundary layer are outlined in Chapter 2.

(b) Energy balance of the total Earth-Atmosphere system

In this section we will use the annual energy balance of the Earth-Atmosphere system to illustrate the linkages between the various energy exchanges and the concept of energy balance. In so doing we will establish both the magnitude of the driving force for the E-A hydrologic cycle (see Section 4(b)) and the energetic context within which all E-A system climates (macro-, meso-, local and micro-) operate.

A schematic depiction of the annual energy balance of the E-A system is given in Figure 1.8. It recognizes the Earth, the Atmosphere and Space as separate sub-systems and places magnitudes on the energy exchanges between them. The E-A system is a *closed* one (i.e. it is closed to the import or export of mass, but it does allow exchange of energy with the exterior (Space). The constant stream of radiant energy emitted by the Sun is the sole input to the system. The magnitude of this input, known as the *solar*

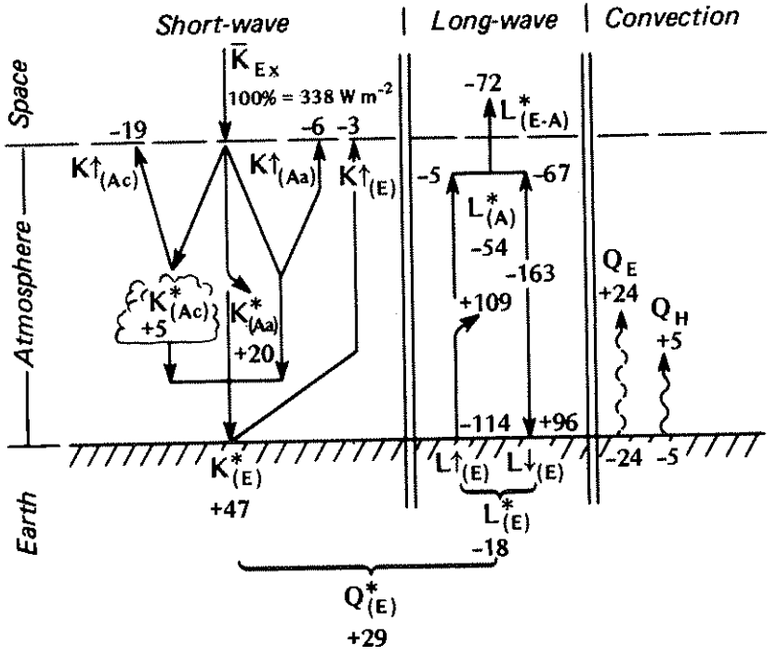

Figure 1.8 Schematic diagram of the average annual solar energy cascade of the Earth-Atmosphere system. Values are expressed as percentages of the average annual extra-terrestrial solar radiation ($\bar{K}_{Ex}$ = 342 W m^{-2}) (data from Rotty and Mitchell, 1974).

constant (I_0), is 1367 W m^{-2} (Wehrli, 1985). It is the value observed outside the Atmosphere on a plane surface placed normal to the solar beam. This represents a practical upper limit for short-wave radiation in the E-A system because the depletion of the Atmosphere is not included and the definition includes the ideal orientation of the receiving surface (i.e. in equation 1.9 $\cos\Theta = 1$). When averaged over the top of the Atmosphere for one year, the spatial mean input ($\bar{K}_{Ex}$) is exactly $I_0/4$ = 342 W m^{-2} (29·5 MJ m^{-2} day^{-1}). In Figure 1.8 all fluxes are represented as percentages of this value. Over the period of a year exactly the same amount of energy must be lost from the E-A system to Space. If this were not so the system would experience a net energy gain or loss, resulting in a net storage change and a rise or fall of the average E-A system temperature (i.e. a climatic shift). Equally, if the sub-systems were not in balance the system would be in disequilibrium. By tracing the energy pathways we will see how balance is achieved.

In the Atmosphere clouds reflect about 19% of $\bar{K}_{Ex}$ back to Space ($K\uparrow_{(Ac)}$) and absorb about 5%($K^*_{(Ac)}$). Atmospheric constituents scatter and reflect

about 6% to Space ($K\uparrow_{(Aa)}$) and absorb about 20%($K^*_{(Aa)}$). The remainder of the original beam is transmitted to the Earth's surface where approximately 3% is reflected to Space ($K\uparrow_{(E)}$) and the remaining 47% is absorbed ($K^*_{(E)}$). Thus, in summary, the solar radiation input is disposed of in the following manner:

$$\bar{K}_{Ex} = K\uparrow_{(Ac)} + K\uparrow_{(Aa)} + K^*_{(Ac)} + K^*_{(Aa)} + K\uparrow_{(E)} + K^*_{(E)}$$
$$100 = 19 + 6 + 5 + 20 + 3 + 47$$

Atmospheric reflection; Atmospheric absorption; Earth reflection; Earth absorption

Three basic features of the short-wave radiation portion of the balance emerge. First, 28% of the E-A input is reflected to Space and does not participate further in the E-A system energy balance. Secondly, only 25% of the input is absorbed by the Atmosphere. Thus, as noted earlier, the Atmosphere is semi-transparent to short-wave radiation and consequently is not greatly heated by it. Thirdly, almost one-half (47%) of the input is absorbed at the Earth's surface. This considerable amount of energy is converted from radiation into thermal energy which warms the surface.

The Earth's surface emits long-wave radiation in accord with equation 1.4. Given that most natural surfaces have emissivities close to unity (Table 1.1), and that the Earth's mean annual temperature is approximately 288 K, this results in an upward emission ($L\uparrow_{(E)}$) of 114% of $\bar{K}_{Ex}$. This apparent anomaly is possible because the Atmosphere blocks the loss of $L\uparrow_{(E)}$ and forces the surface temperature above the value it would otherwise have with no Atmosphere. In fact only 5% is lost directly to Space, the remaining 109% being absorbed by the Atmosphere. It should also be noted that the Earth emits long-wave over its entire surface area, but only receives short-wave over the sunlit hemisphere. The Atmosphere emits long-wave radiation to Space (67%) and to the Earth's surface, $L\downarrow_{(E)}$ (96%), amounting to a total output of 163%.

Let us summarize the radiation budgets of the E-A system and the Earth and Atmosphere sub-systems. The whole E-A system is in radiative equilibrium because the solar input (100%) is matched exactly by the sum of the short-wave scattering and reflection (19 + 6 + 3 = 28%) and the long-wave emission from Earth and its Atmosphere (5 + 67 = 72%).

The sub-systems are not in equilibrium. The Earth's surface receives a net input of short-wave radiation ($K^*_{(E)}$) equivalent to 47% of $\bar{K}_{Ex}$, but experiences a net loss of long-wave radiation ($L^*_{(E)}$) of 18% (because it emits 114% to the Atmosphere but receives 96% in return). Thus the net all-wave radiation budget for the Earth ($Q^*_{(E)}$) is positive and represents 29% (47 − 18) of the original extra-terrestrial input. In the case of the Atmosphere it gains 25% as $K^*_{(A)}$ due to absorption by clouds and atmos-

pheric constituents (see equation 1.7), but loses 54% as $L^*_{(A)}$ (because although it absorbs 109% from the surface, it emits 163% to Space and back to the surface). Thus the net all-wave radiation budget of the atmosphere ($Q^*_{(A)}$) is −29% (25 − 54).

Therefore the Earth has an annual radiant energy surplus of 29% and the Atmosphere has an annual radiant energy deficit of the same amount. This does not mean there is a balance. Considering their respective physical and thermal properties, this situation would result in the Earth warming up at the rate of approximately 250°C day^{-1} and the Atmosphere cooling at approximately 1°C day^{-1}! Such heating and cooling rates are not observed because convection transports energy equivalent to the radiative surplus of the Earth into the Atmosphere thereby offsetting its deficit; 5% of the exchange is as sensible heat (Q_H) and 24% is as latent heat (Q_E). For completeness we should note that conduction does not appear in Figure 1.8 because over the annual time period net sub-surface storage is zero.

(c) Diurnal energy balance at an 'ideal' site

In Section 1 it was noted that boundary layer climates respond to processes operating on time scales of less than one day. This section outlines the most important general features of the diurnal energy regime at a given site. This is best accomplished by considering the case of an 'ideal' site. Such a location presents the minimum complication being horizontal, homogeneous and extensive. These constraints ensure that surface/atmosphere fluxes are spatially uniform and confined to the vertical direction. To minimize fluctuations in the time domain only cloudless conditions are considered initially, so that the solar input is a smooth wave. The surface is a flat, moist, bare soil (or short grass) located in the mid-latitudes in the warm season. In Part II of the book these constraints are removed.

Figure 1.9 shows the diurnal variation of the important radiation budget components at a site meeting our 'ideal' criteria, and the accompanying table summarizes the daily energy totals. The pattern of incoming shortwave radiation ($K\downarrow$) is controlled by the azimuth (Ω) and zenith (Z) angles of the Sun relative to the horizon, with a maximum at local solar noon. (Definitions of these angles and methods to calculate them for any latitude, time of year and hour are given in Appendix A1 together with information concerning the path of the Sun across the sky and the effect of horizon obstruction.)

In the middle of a cloudless day the proportion of $K\downarrow$ arriving as diffuse radiation is anywhere from 10 to 25% depending on the amount of water vapour haze; in smoggy urban and industrial areas it will be even greater. Early and late in the day the diffuse proportion also increases due to the greater path length of the Sun through the Atmosphere (see Figure 1.12).

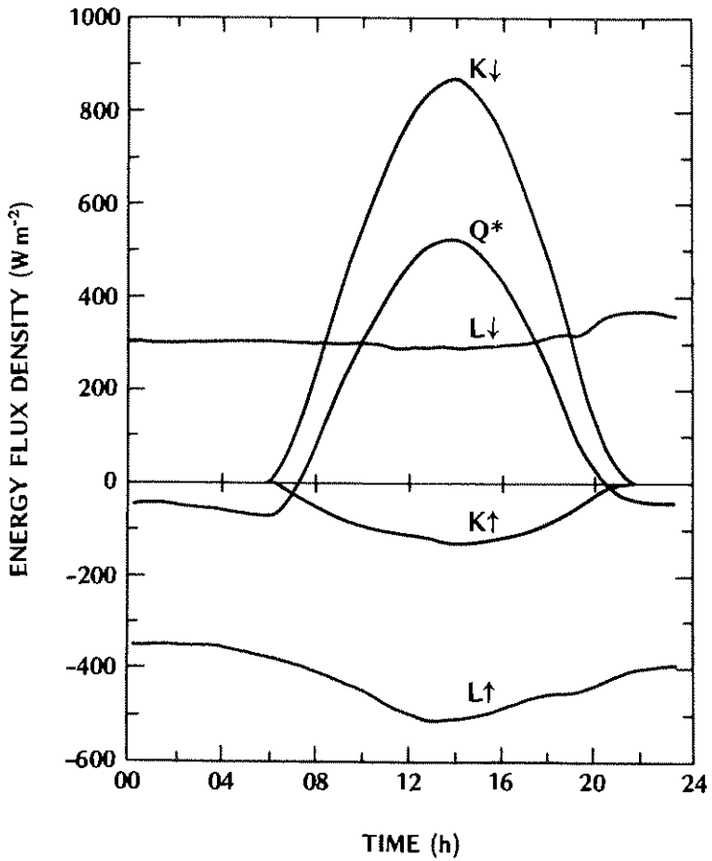

Figure 1.9 Radiation budget components for 30 July 1971, at Matador, Saskatchewan (50°N) over a 0·2 m stand of native grass. Cloudless skies in the morning, increasing cloud in the later afternoon and evening (after Ripley and Redmann, 1976). (*Note* – In the text no signs have been given to individual radiation fluxes, only to net fluxes (K^*, L^* and Q^*). However, in figures such as this radiative inputs to the surface ($K\downarrow$, $L\downarrow$) have been plotted as positive, and outputs ($K\uparrow$, $L\uparrow$) as negative to aid interpretation.) The following table gives the radiation totals for the day (MJ m^{-2} day^{-1}).

$K\downarrow$	27·3	$L\downarrow$	27·5
$K\uparrow$	4·5	$L\uparrow$	36·8
K^*	22·7	L^*	−9·3
α†	0·16	Q^*	13·4

† Dimensionless

In a relatively clean atmosphere approximately 50% of $K\downarrow$ is in the visible portion of the electromagnetic spectrum.

The short-wave radiation reflected from the surface ($K\uparrow$) depends on the amount of incident radiation ($K\downarrow$) and the surface albedo (α, see Table 1.1, p. 12):

$$K\uparrow = K\downarrow(\alpha) \tag{1.11}$$

Although α is not a perfect constant through a day (e.g. see p. 86 and Figures 3.12 and 4.14) to a first approximation, it is reasonable to expect $K\uparrow$ to be a reduced mirror-image of $K\downarrow$ (Figure 1.9). Given that the surface is opaque to short-wave radiation (i.e. $\Psi_{short} = 0$), the portion of $K\downarrow$ that is not reflected is absorbed, so the net short-wave radiation (K^*) is:

$$\begin{aligned} K^* &= K\downarrow - K\uparrow \\ &= K\downarrow\ (1 - \alpha) \end{aligned} \tag{1.12}$$

Therefore in our example, since $\alpha = 0{\cdot}16$, $K\uparrow$ would describe a curve with positive values of about $0{\cdot}84K\downarrow$ in Figure 1.9.

The incoming long-wave radiation emitted by the atmosphere ($L\downarrow$) in the absence of cloud depends upon the bulk atmospheric temperature and emissivity (which itself depends on the distributions of temperature, water vapour and carbon dioxide) in accord with the Stefan–Boltzmann Law (equation 1.4). Neither of these properties fluctuates rapidly and hence $L\downarrow$ is almost constant through the day (see Figure 1.9; note the increase of $L\downarrow$ between 18 and 24 h is discussed on p. 26).

The outgoing long-wave radiation from the surface ($L\uparrow$) is similarly governed by its temperature and emissivity. If the surface is a full radiator ($\varepsilon_0 = 1$) the output is given by equation 1.3, but if ε_0 is less than unity:

$$L\uparrow = \varepsilon_0\sigma T_0^4 + (1 - \varepsilon_0)\, L\downarrow \tag{1.13}$$

The second term on the right accounts for the amount of $L\downarrow$ that is reflected (see equation 1.8). For most surfaces the adjustment is small. Because the values of T_0 and ε_0 are greater than their atmospheric counterparts, and because T_0 varies considerably through the day, the value of $L\uparrow$ is both greater in magnitude and more variable than $L\downarrow$.

The difference between the two long-wave fluxes is the surface net long-wave radiation budget (L^*):

$$L^* = L\downarrow - L\uparrow \tag{1.14}$$

The value of L^* (not plotted in Figure 1.9) is usually negative, and relatively small (75 to 125 W m^{-2}) if the surface and air temperatures are not significantly different. If the surface is considerably warmer than the air (e.g. as in Figure 7.3, p. 233) L^* may be much larger. The diurnal course of L^* is usually in phase with $L\uparrow$.

The net all-wave radiation (Q^*) is the most important energy exchange because for most systems it represents the limit to the available energy source or sink. The daytime surface budget is the sum of the individual short- and long-wave streams:

$$\begin{aligned} Q^* &= K\downarrow - K\uparrow + L\downarrow - L\uparrow \\ &= K^* + L^* \end{aligned} \tag{1.15}$$

and, at night solar radiation is absent so that:

$$\begin{aligned} Q^* &= L\downarrow - L\uparrow \\ &= L^* \end{aligned} \tag{1.16}$$

Thus the typical diurnal course of Q^* (Figure 1.9) involves a daytime surface radiant surplus when the net short-wave gain exceeds the net long-wave loss; and a nocturnal surface deficit when the net long-wave loss is unopposed by solar input. At a given location the terms $K\downarrow$ and $L\downarrow$ are unlikely to show significant spatial variability because they are governed by large-scale atmospheric, or Earth–Sun geometric relationships. On the other hand $K\uparrow$ and $L\uparrow$ are governed by sensitive site specific factors (i.e. $K\uparrow$ by α; $L\uparrow$ by T_0 and ε_0). Thus it is these terms which govern the differences in radiation budget (Q^*) between surfaces in the same local region. In conclusion it should be noted that the range of Q^* values over different surfaces is damped somewhat by a built-in negative feedback mechanism. The range of natural surface ε_0 values is small (Table 1.1) and hence differences in Q^* effectively depend upon the values of α and T_0. A surface with a low albedo will absorb well, but unless it possesses channels for rapid heat dissipation this will result in a high surface temperature. Thus the large K^* gain will be matched, at least in part, by a large L^* loss.

Appendix A_2 provides examples of the currently utilized methods (measurement and calculation) for the determination of the surface radiation balance fluxes, and the relevant surface radiative properties.

The net all-wave radiation flux is not only the end result of the radiation budget but also the basic input to the surface energy balance. Figure 1.10a shows the typical diurnal variation of the components of the surface energy balance at an 'ideal' site, and its table summarizes the daily energy totals. At any given time it can be seen that any surface radiative imbalance is accounted for by a combination of convective exchange to or from the atmosphere, either as sensible (Q_H) or latent heat (Q_E), and conduction to or from the underlying soil (Q_G). Thus the surface energy balance is:

$$Q^* = Q_H + Q_E + Q_G \tag{1.17}$$

The sign convention employed in Figure 1.10a (and throughout the remainder of the book) is that non-radiative fluxes directed away from a

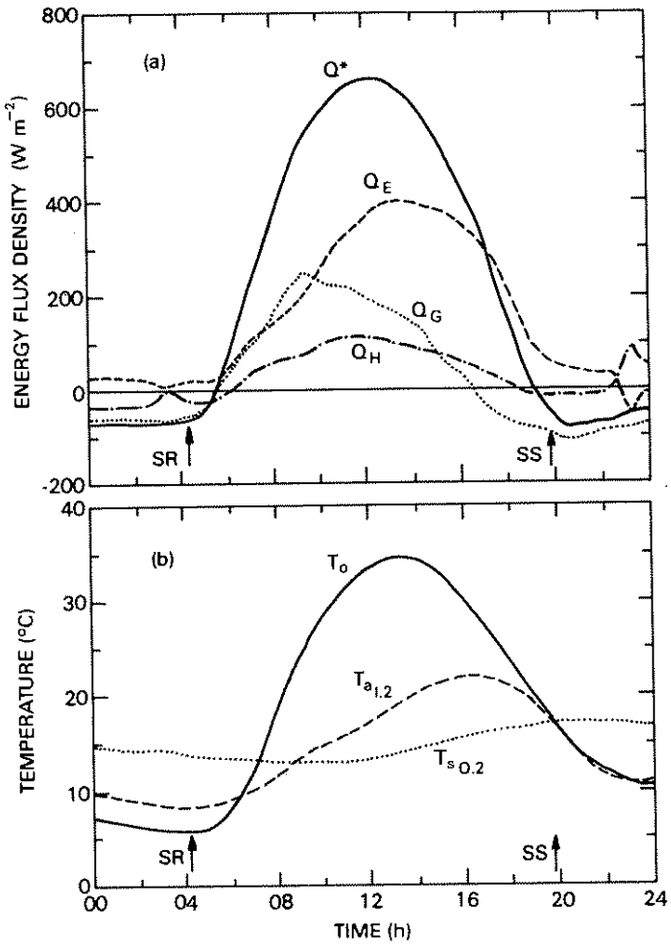

Figure 1.10 (a) Energy balance components for 30 May 1978 with cloudless skies at Agassiz, B.C. (49°N) for a moist, bare soil, and (b) temperatures at the surface, in the air at a height of 1·2 m and in the soil at a depth of 0·2 m (after Novak and Black, 1985). The following table gives the energy totals for the day (MJ m^{-2} day^{-1}).

Energy balance		Derived terms	
Q^*	18·0	β	0·17
Q_H	2·3	Q_E/Q^*	0·75
Q_E	13·4	E(mm)	5·45
Q_G	2·3		

surface (or system) are positive. Thus the terms on the right-hand side of equation 1.17 are positive when they represent losses of heat for the surface (or system), and negative when they are gains. On the left-hand side Q^* is positive as a gain and negative when a loss. When both sides of the equation are positive it describes how the available radiative surplus is partitioned into sub-surface and atmospheric energy sinks; and this is usually the situation by day. When both sides are negative the equation states how the surface radiative deficit is partitioned between heat gain from available sub-surface and atmospheric sources; and this is the normal nocturnal situation. The flux of momentum is an exception to this convention (see Chapter 2).

The exact partitioning of the radiative surplus or deficit (between Q_H, Q_E and Q_G) is governed by the nature of the surface, and the relative abilities of the soil and atmosphere to transport heat. The particular apportionment arrived at by a surface is probably the most important determinant of its microclimate.

The diurnal course of Q^* in Figure 1.10a is very similar to that of Figure 1.9. *Under the given conditions* the daytime Q^* is dissipated as Q_E, Q_G and Q_H in descending order of importance. The dominant role of Q_E is a result of the free availability of soil moisture for evaporation at this irrigated site. If water became more restricted we might expect the role of Q_E to drop, and of Q_H to rise. No matter which dominates it is clear that convection is the principal means of daytime heat transport away from the interface.

At night on the other hand the situation is reversed. The nocturnal Q^* loss is most effectively replenished by conduction upwards from the soil, and the convective contribution is least effective from Q_E. The essential difference between the two convective situations is due to the fact that by day free convection is enhanced, but by night it is damped by the atmospheric temperature stratification (p. 51). The size of Q_G is not greatly different between day and night. In fact, although Q_G is a significant energy source, or sink, on an hourly basis, when integrated over the full day its net effect is not large (see the table accompanying Figure 1.10). In summer the daytime storage slightly exceeds the nocturnal output and the soil gradually warms. The reverse is true in winter.

Figure 1.11 provides a convenient schematic summary of the terms involved in the surface radiation and energy budgets of an 'ideal' site.

Before concluding this section a few remarks should be added concerning the effects of cloud, and non-uniform surface properties, upon the 'ideal' situation described above. Clouds exert a major influence on the exchanges of short- and long-wave radiation. The surface receipt of $K\downarrow$ is reduced because of cloud absorption and the reflection from cloud tops, and with partly cloudy skies short-term variability becomes great. For example, in

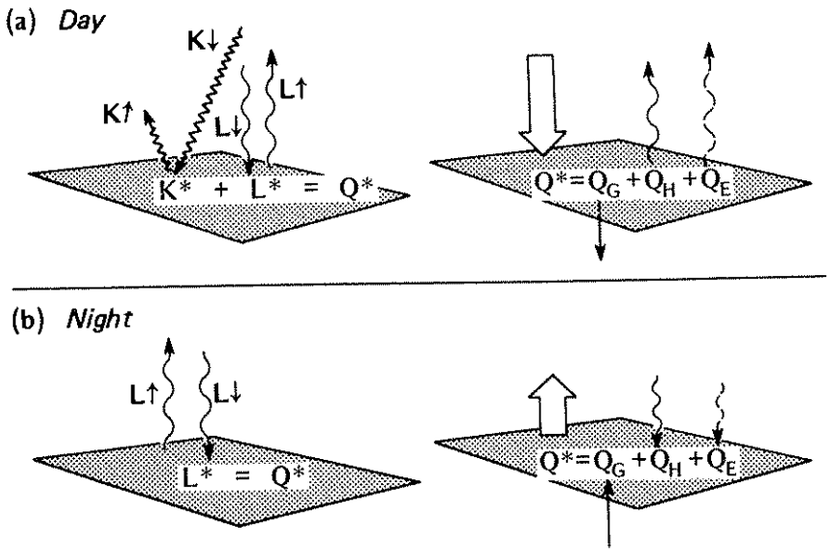

Figure 1.11 Schematic summary of the fluxes involved in the radiation budget and energy balance of an 'ideal' site, (a) by day and (b) at night.

the afternoon of the day shown in Figure 1.12 the very rapid fluctuations in $K\downarrow$ are due to the almost complete elimination of S by cloud. At the same time there are relative increases in D. Notice also the short-term bursts of $K\downarrow$ that *exceed* the cloudless values by about 5–10%. These occur when the recording station is in receipt of direct-beam and diffuse sky radiation as normal plus reflection from the sides of isolated cumulus clouds in the vicinity. With a complete overcast of low, thick cloud $K\downarrow$ can be reduced to 10% of the cloudless value and beam irradiation is completely eliminated. Contrary to the cloudless case, D is greater from the zenith than from near the horizon.

The surface long-wave budget is profoundly affected because clouds are almost black bodies (p. 15) and thus absorb and emit very efficiently. Clouds therefore absorb much of $L\uparrow$ from the surface and re-emit it back so that $L\downarrow$ is enhanced, and L^* reduced. The arrival of cloud explains the abrupt increase of $L\downarrow$ noted in Figure 1.9 after 18 h. The cloud emission depends on the cloud-base temperature, therefore the effect of Stratus (low, relatively warm) is much greater than Altus or Cirrus (high, cold) cloud. The net result of cloud is to damp the diurnal surface radiation budget variation, and serves to reduce the diurnal temperature range. This explains why cloudy weather is associated with comparatively uniform temperatures because daytime solar heating and night-time long-wave cooling are both reduced.

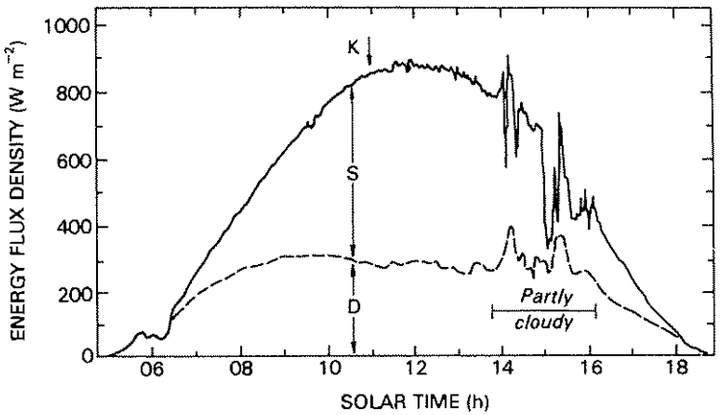

Figure 1.12 Variation of incoming solar radiation ($K\downarrow$) on a very hazy day (10 August 1975) in central Illinois (39°N), including the distinction between direct-beam (S) and diffuse radiation (D) (modified after Wesely, 1982).

If the site is not sufficiently extensive it is possible that heat exchange can occur between it and upwind surfaces possessing different energy partitioning. For example, if our grass site was downwind of a hot dry soil surface it is possible that horizontal airflow could carry air with greater sensible heat content (and therefore higher temperature) across the grass. This would alter the atmospheric conditions and give rise to an adjustment in the surface energy fluxes. In the example used it would tend to suppress the local surface value of Q_H and to augment Q_E (this is explained more fully in Chapter 5). The net horizontal convective heat transport (both sensible and latent) is called *advection* (ΔQ_A). Unless specifically noted it may be assumed that the surface climates outlined in Part II are advection-free. In reality this is rarely completely true.

(d) Atmospheric motion

Horizontal temperature variations in the E-A system give rise to horizontal pressure differences, which result in motion (winds). In this way thermal energy from the solar energy cycle is converted into the kinetic energy of wind systems. The energy then participates in the *kinetic energy* cascade involving the transfer of energy to increasingly small scales of motion by turbulence. This is the sequence depicted in Figure 1.1. Kinetic energy enters the cascade at a size-scale governed by the forces generating the motion. The energy is then passed down to smaller-sized eddies until it eventually reaches the molecular scale and is dissipated as heat (i.e. it returns to the thermal portion of the solar energy cycle). This energy does

not appear in Figure 1.8 because on an annual basis there is a balance between kinetic energy production and dissipation.

In the boundary layer we are concerned both with motion generated on the micro- and local scales, and with the modification of existing airflow generated on scales larger than those of the boundary layer. In the first category we are concerned with wind systems generated by horizontal thermal differences in the boundary layer. These local scale thermal winds are especially prevalent across the boundaries between contrasting surface types. Examples include the breezes occurring at land/sea (lake), mountain/valley, forest/grassland, and urban/rural interfaces. In the second category we are concerned with the role of surface roughness in shaping the variation of wind speed with height, and with the way in which uneven terrain (e.g. hills and valleys) and isolated obstacles (e.g. a tree or a building) perturb existing flow patterns. All of these aspects are considered in Chapter 5.

4 MASS BALANCES

(a) Properties of water

Water possesses a number of unusual properties which make it an important climatological substance. One important thermal property is its high *heat capacity* (see p. 36 and Table 2.1, p. 44). This effectively means that in comparison with most other natural materials it takes much more energy input to cause a similar rise in the temperature of water. Equally, subtraction of energy does not cause water to cool as rapidly. This property makes water a good energy storer, and a conservative thermal influence.

Water is the only substance that exists in all of its states at temperatures normally encountered in the E-A system. In changing between ice, water and water vapour, latent heat is taken up or liberated and as a result the energy and water balances become enmeshed. The energy required to effect a change between the ice and water phases (i.e. consequent upon melting or freezing) is 0·334 MJ kg^{-1} at 0°C, and is called the *latent heat of fusion* (L_f). The change between liquid water and water vapour (i.e. consequent upon evaporation or condensation) at 0°C requires 2·50 MJ kg^{-1} which is almost 7·5 times more energy. This is the value of the latent heat of vaporization (L_v), and at 10°C it is 2·48, at 20°C 2·45 and at 30°C 2·43 MJ kg^{-1} (see Appendix A3, p. 393). In the event that the water changes directly between the ice and vapour phases (i.e. sublimates) the *latent heat of sublimation* (L_s) is the algebraic sum of L_f and L_v, and at 0°C it is 2·83 MJ kg^{-1}. To gain some measure of the energy amounts involved it should be realized that the energy locked-up in evaporating 1 kg of water is roughly equivalent to that necessary to raise 6 kg of water from 0°C to 100°C.

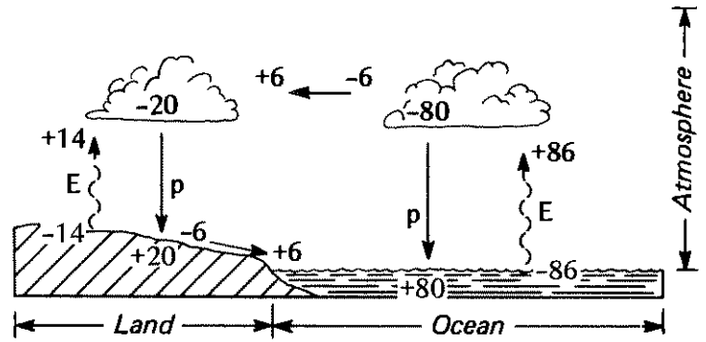

Figure 1.13 Schematic diagram of the average annual hydrologic cycle of the Earth-Atmosphere system. Values expressed as percentages of the mean annual global precipitation of 1040 mm (data from Chow, 1975).

(b) Water balance

The annual global cycle of water in the E-A system is given in Figure 1.13. All quantities of water are represented as percentages of the mean annual global precipitation, which is approximately 1040 mm. Utilizing energy provided by the energy balance (Figure 1.8) water is evaporated from open water surfaces (oceans and lakes) and the soil, and is transpired from vegetation. The composite loss of water to the air from all sources is called the *evapotranspiration* (E). The water vapour is carried up into the Atmosphere by unstable air masses, and mechanical convection. Eventually the vapour is cooled to its dew-point (p. 64), and it condenses as a cloud droplet, or ice crystal. Under favourable conditions the cloud droplets or crystals may grow to a size where they can no longer be held in suspension and they fall to the Earth as *precipitation* (p). Near the surface water may also be deposited by direct condensation or sublimation as dew, hoar frost, and rime, or be impacted as fog-drip. Over land areas p is greater than E, and the excess is transported as streamflow to the oceans where E is greater than p (Figure 1.13). So that for the Land and Ocean sub-systems their annual water balance may be written:

$$p = E + \Delta r$$

where, Δr – *net runoff* (i.e. the net change in runoff over a distance). This term may have a positive or negative sign. It is positive if more water leaves than arrives as is normally the case on sloping land. Δr is negative when surface flow leads to accumulation of water such as when lake levels rise. For the total E-A system on an annual basis the balance is even simpler:

$$p = E$$

because the system is closed to the import or export of mass and hence all horizontal transfers (such as runoff or ocean currents) are internal, and the net storage change for the system is zero.

We will accept the macro-scale conditions as given, and concentrate on small-scale surface/atmosphere interaction over relatively short time periods. Let us return to the case of our 'ideal', or short grass, site with a moist soil on level terrain. If we consider the water exchanges through the surface plane (Figure 1.14a) then we can formulate the surface water balance equation as:

$$p = E + f + \Delta r \tag{1.18}$$

where f-infiltration to deeper soil layers. Normally f is positive due to gravity. Although less common f can be negative, for example, where a ground water table intersects a hillslope leading to spring seepage. Infiltration is not easily determined so for practical purposes it is better to consider a column (Figure 1.14b) which extends from the surface to a

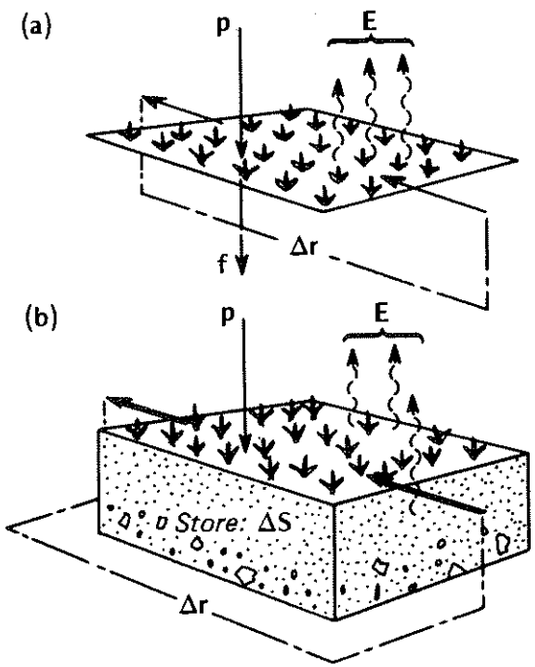

Figure 1.14 Diagrammatic representation of the components of the water balance of (a) a natural surface, and (b) a soil-plant column.

depth where significant vertical exchanges are absent (i.e. where $f \rightarrow 0$), then the water balance is given by:

$$p = E + \Delta r + \Delta S \tag{1.19}$$

where ΔS – the net change in *soil moisture content*. The soil moisture content is a measure of the mass of water stored in a soil in the same way as soil temperature is a measure of the soil heat content. Equation 1.19 shows how the water storage in the system is dependent upon the water input which is usually mainly p, and the water output via E and Δr. Input could also be supplied by irrigation which would require an additional term on the left-hand side of equation 1.19, or it could be as dewfall (i.e. convective transfer from the air to the surface $-E$). Evapotranspiration consists of evaporation of free surface water (e.g. puddles), and soil pore water, and water transpired from vegetation.

The time scale over which equation 1.19 is valid proves awkward if we are properly to integrate it with the surface energy balance (equation 1.17) on time periods of a day or less. This arises because the input/output processes are fundamentally different in nature. Precipitation usually occurs in discrete, short-period bursts, whereas evaporation is a continuous and variable function. Thus, for example, during periods with no precipitation water input is zero but the soil moisture store is being almost continually depleted by evapotranspiration. In these circumstances equation 1.19 effectively reduces to:

$$E = \Delta S \tag{1.20}$$

because Δr is negligible on level terrain. Therefore, unlike the annual situation where net water storage is zero, on the short time-scale ΔS is non-zero and very important.

Soil moisture is significant in surface energy balance considerations because it is capable of affecting radiative, conductive and convective partitioning. For example, the addition of moisture can alter the surface albedo thereby changing K^* and Q^*. Equally the thermal properties of a soil are changed by adding water, so that heat transfer and storage are affected. Most important however are the potential latent heat effects of soil moisture.

The common term in the water and energy balance equations is evaporation. The fluxes of mass (E) and energy (Q_E) associated with evaporation are linked by the relation:

$$Q_E = L_v E \tag{1.21}$$

where the units of E are kg m^{-2} s^{-1} (mass transport through unit surface area in unit time). Therefore if the energy scale of Figure 1.10 were divided by L_v the curve of Q_E becomes the diurnal course of E.

When temperatures are at or below 0°C and the change of water phase

is to or from the solid state (ice), the equivalent expression is:

$$\Delta Q_M = L_f M \qquad (1.22)$$

Here ΔQ_M is the energy flux density needed to melt water at the mass flux density M (kg m^{-2} s^{-1}), or it is the energy flux density that is released upon freezing.

For hydrologic purposes it is convenient to express the mass flux densities E and M in terms of an equivalent depth of water (millimetres) over the period of concern (usually an hour or a day). They are then consistent with the normal units of precipitation. Details of the conversion factors involved are given in Appendix A4e (p. 398). The simple conversion 1 mm evaporation = 2·45 MJ m^{-2} has been applied to the daily total value of Q_E in the table accompanying Figure 1.10 to yield the daily water loss in millimetres.

It is also satisfying to note that conversion of the Q_E annual energy term in Figure 1.8 to an equivalent height of water evaporated gives a value of E very close to that in Figure 1.13. Thus loss of water to the air not only depletes the mass store (soil moisture) but also the energy store (soil and air temperature) as a result of taking up latent heat. Condensation operates in the reverse sense by adding to both the mass and energy stores. Melting and freezing are energetically less significant, but still of importance especially in soil climate.

The measures of soil moisture content, and the processes of soil moisture movement and evaporation, are outlined in Chapter 2.

(c) Other mass balances

The cycles of energy and water are by far the most important in explaining surface climates, but it should be noted that there are others operating in the E-A system on similar space and time scales. Examples include the cycles of carbon, nitrogen, oxygen and sulphur. Of these the CO_2 portion of the carbon cycle is of most immediate interest to this book because it interacts with both solar energy and water in the process of photosynthesis. This is dealt with in Chapter 4 and an example of the diurnal flux of CO_2 is given in Figure 4.10.

2 Physical basis of boundary layer climates

1 EXCHANGES AND CLIMATIC RESPONSES NEAR SURFACES

This section opens by considering the concept of a 'surface' and how exchanges at this interface produce climatic effects. It then considers the corresponding relations for a volume rather than a plane. Finally, it explains how surface influences are conveyed to the boundary layers adjacent to the surface. For simplicity the arguments will be restricted to the case of heat exchange and temperature near an 'ideal surface'. The generality of these concepts will become apparent in the rest of the chapter which includes the cases of momentum and mass exchange and their related climatic effects.

(a) The 'active' surface

Frequent reference has already been made to the Earth's 'surface'. In technical terms a surface is a plane separating two different media. Of itself it contains no energy or mass, but it is the site of very important energy and mass exchange and conversion.

Problems arise in determining the position of the surface in many natural environments. For example, the surface may be in motion (e.g. water), or be semi-transparent to radiation (e.g. ice, snow, water, plant cover), or be composed of many elemental surfaces (e.g. leaves on a tree), or may be serrated by large roughness units (e.g. trees in a forest, buildings in a city). For climatic purposes we define the 'active' surface as the principal plane of climatic activity in a system. This is the level where the majority of the radiant energy is absorbed, reflected and emitted; where the main transformations of energy (e.g. radiant to thermal, sensible to latent) and mass (change of state of water) occur; where precipitation is intercepted; and where the major portion of drag on airflow is exerted.

Where appropriate, the position of the active surface will be identified for each of the environments treated in this book.

Viewed in detail no surface is flat, but is composed of some form of roughness element, therefore some degree of simplification is necessary as a working basis. For climatic purposes it seems best to retain a pragmatic concept of the active surface which is adjustable to allow for the scale of inquiry and the entity under study.

The location of the surface and the relationship between the surface energy balance and the surface temperature (T_0) is relatively simple for the case of a flat bare soil such as that in Figure 1.10 (p. 24). At all times equation 1.1 is satisfied: for most of the daytime the input to the system is entirely radiatively (Q^*) driven. After about 16 h some asymmetry in the temperature curve is introduced by the reversal of the soil heat flux density (Q_G). This pattern, with a sharper warming than cooling limb to the temperature curve, is typical. The magnitude of the warming is a complex result of the thermal and moisture properties of the soil (especially the thermal admittance, p. 46) and the state of turbulence and air mass properties of the air. The nocturnal cooling is also radiatively driven with a further drain due to some evaporation. Overall the course of the surface temperature wave (including the time of the peak) is closely linked to the surface radiation budget.

(b) Exchange in a volume

The formulation of the surface energy balance (equation 1.17):

$$Q^* = Q_H + Q_E + Q_G$$

is consistent with equation 1.1 (Energy Input = Energy Output) because the surface is considered to be a massless plane which itself has no heat content. In many of the systems we are about to analyse it is more appropriate to view the energy balance as relating to a volume (or layer). It is then necessary to include changes of energy storage (ΔQ_S) as described by equation 1.2 (Energy Input − Energy Output − Energy Storage Change = 0), so that we should write:

$$Q^* = Q_H + Q_E + Q_G + \Delta Q_S \qquad (2.1)$$

The term ΔQ_S arises because of energy absorption or release by the volume. This means that the input and output of *at least* one of the individual fluxes (Q^*, Q_H, Q_E and Q_G) do not balance. This concept is illustrated in Figure 2.1 where the arrows represent fluxes of energy into (Q_{in}), and out of (Q_{out}), the system volume. The length of the arrows represents the magnitude of the flux. There are three possibilities:

(i) Q_{in} exceeds Q_{out} – from simple systems considerations if the input of energy exceeds the output then there must be a net energy storage gain ($+\Delta Q_S$) in the volume. This situation is one of *flux convergence*, and will result in a warming of the volume (Figure 2.1a). The amount of the temperature change per unit of energy storage change will depend upon the thermal properties of the materials of the volume.

(ii) Q_{in} is less than Q_{out} – if input is less than output the volume must be losing energy, thereby depleting its energy store ($-\Delta Q_S$) and hence cooling. This is the case of *flux divergence* (Figure 2.1b).

(iii) $Q_{in} = Q_{out}$ – if input equals output there is no net change in the energy status of the volume (i.e. $\Delta Q_S = 0$), or its temperature.

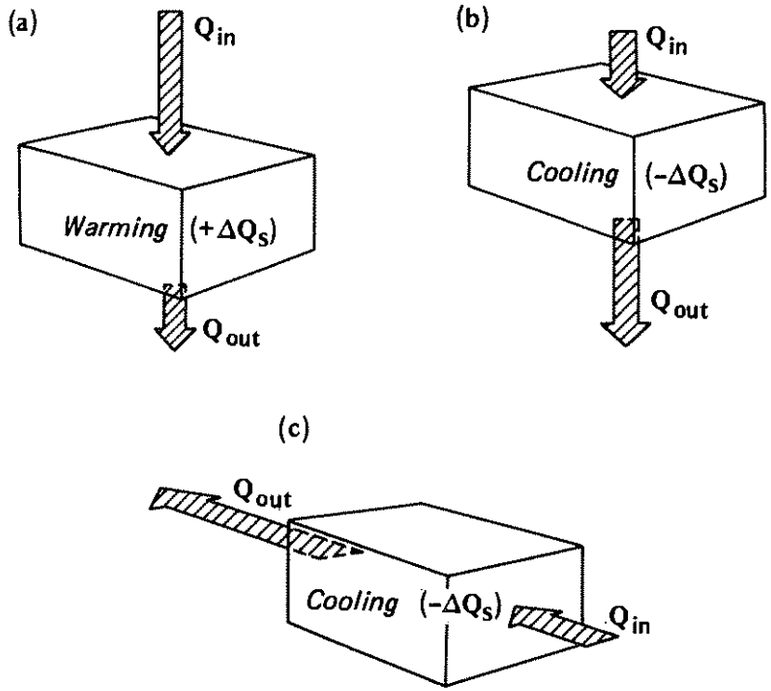

Figure 2.1 Schematic depiction of (a) vertical flux convergence, (b) vertical flux divergence and (c) horizontal flux divergence, in a volume.

The concept of convergences and divergence is more general than depicted in Figure 2.1. For example, the direction of the flux is unimportant, it is the net change in the flux that influences the energy balance of the volume. Convergence and divergence of horizontal fluxes can also contribute to warming and cooling (Figure 2.1c). This is advection (ΔQ_A) and its effects are dealt with in Chapter 5. Thus it is often necessary to consider a full three-dimensional balance. Moreover, the flux arrows in Figure 2.1

could represent a conductive, radiative or convective transport, or any combination of the three.

An example will help to illustrate this rather abstract concept. Imagine that the arrow in Figure 2.1a represents the flux density of sensible heat (Q_G) downward into a volume of soil, typical of daytime conditions. Since the flux density (arrow) emerging from the base of the soil volume is less some of the heat energy has been retained, and the soil would warm due to conductive heat flux convergence.

The actual mean temperature change $\Delta\overline{T}$ is of course proportional to the amount of heat absorbed ($+ \Delta Q_S$) but it also depends upon the thermal properties of the soil. (*Note* – the overbar indicates a time-averaged quantity.) When considering unit mass of the substance, the appropriate property is the *specific heat* (c, with units of J kg^{-1} K^{-1}). Here when dealing with unit volume, the property is the *heat capacity* (C, with units of J m^{-3} K^{-1}), which is defined as the amount of heat (J) necessary to raise unit volume (m^3) of a substance through a temperature change of 1 degree (K). Typical values of c and C are listed in Table 2.1 (p. 44) where it is clear that, compared to most other materials, water requires a large heat input to effect a given change in temperature whereas air requires very little.

We can quantify the case of our hypothetical soil volume by writing:

$$\frac{\Delta Q_S}{\Delta z} = C_s \frac{\Delta \overline{T}_s}{\Delta t} \tag{2.2}$$

which says that the change of heat flux density in the layer Δz (or change of heat flux in the volume) is equal to the product of the heat capacity of the soil and the heating/cooling rate (temperature change over time period Δt). Using realistic midday values of $Q_{in} = 100$ W m^{-2}, $Q_{out} = 10$ W m^{-2}, $\Delta z = 0{\cdot}5$ m, for a dry clay with $C_S = 1{\cdot}42 \times 10^6$ J m^{-3} K^{-1}, after re-arranging the equation we find the warming rate to be:

$$\frac{\Delta \overline{T}_s}{\Delta t} = \frac{\Delta Q_s}{\Delta z \cdot C_s} = \frac{90 \text{ J m}^{-2} \text{ s}^{-1}}{0{\cdot}5 \text{ m} \times 1{\cdot}42 \times 10^6 \text{ J m}^{-3} \text{ K}^{-1}}$$

$$= 1{\cdot}27 \times 10^{-4} \text{ K s}^{-1}$$

which is about 0·46 K h^{-1}.

This concept of flux convergence and divergence in a volume (or a layer if the substance is horizontally uniform) is crucial to an understanding of how boundary layer climates are formed. It lies at the heart of how exchanges of entities such as heat, mass and momentum are related to their associated climatological properties of temperature, water vapour, wind speed, etc. The entity, the processes involved in its exchange, the substance of the medium and the direction of the exchange can all be different from the preceding example, but the principle remains the same.

(c) Exchange in boundary layers

As noted in Chapter 1, it is appropriate to divide the soil-atmosphere system into a series of boundary layers aligned approximately parallel to the active surface. Here we will set out their nature in more detail.

(i) Sub-surface layer

The influence of the active surface extends down into a relatively shallow layer of the sub-strate. Confining ourselves to the semi-solid case of soil for the moment, the interaction between the active surface and this layer is mostly confined to molecular exchange. If we again use the case of heat flow and temperature we can note that heat will flow from areas of high to lower temperature. The magnitude of the flux will be proportional to the temperature difference over the layer (more accurately to the mean heat concentration gradient, C_s ($\Delta\overline{T}_s/\Delta z$)), and the constant of proportionality is called the molecular diffusion coefficient (or *molecular diffusivity*) because the transfer of energy is due to molecular collisions transferring kinetic energy. Thus in mathematical form:

$$Q_G = - \kappa_{Hs} C_s \frac{\partial \overline{T}}{\partial z} \tag{2.3}$$

where κ_{Hs} is the *soil thermal diffusivity* (m^2 s^{-1}). The negative sign indicates that the flux is in the direction of decreasing concentration. This *flux-gradient* form of equation, i.e.:

$$\begin{matrix}\text{Flux} \\ \text{of an Entity}\end{matrix} = \begin{matrix}\text{Ability to} \\ \text{Transfer}\end{matrix} \times \begin{matrix}\text{Gradient of a} \\ \text{Relevant Property}\end{matrix}$$

will re-occur throughout our discussions including other media than soil and other entities than heat.

Because the active surface is the site of greatest energy absorption by day and depletion by night, it is also where the greatest thermal response is found. The effects diminish with distance away from the interface down into the soil. The surface energy balance and temperature wave (see Figure 1.10) establish a temperature gradient and soil heat flux directed downwards by day and upwards at night. The size of both diminish with distance away from the interface giving the vertical distribution (*profile*) of soil temperature illustrated in Figure 2.2. Similarly, the amplitude of the temperature wave decreases, and the time taken for the wave to penetrate increases, with depth (compare T_0 and $T_{s_{0\cdot2}}$ in Figure 1.10b).

(ii) Laminar boundary layer

Immediately above the surface is the laminar boundary layer. It is the thin skin (only a few millimetres) of air adhering to all surfaces within which

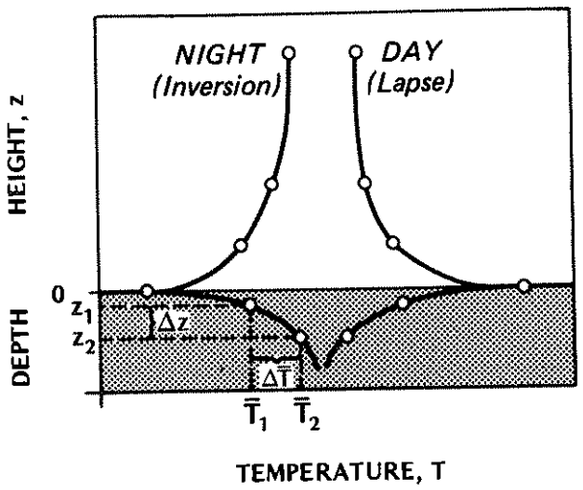

Figure 2.2 Idealized mean profiles of air and soil temperature near the soil/atmosphere interface in fine weather.

the motion is *laminar* (i.e. the streamlines are parallel to the surface with no cross-stream component). The connotation is that adjacent layers (laminae) of the fluid remain distinct and do not intermix. The flow is therefore smooth in appearance. The slow flow of water from a laboratory faucet, or of smoke from a smouldering cigarette or taper in a still room, are laminar initially. Figure 2.3a shows how a boundary layer grows with distance over a flat plate (see also Figures 4.6 and 6.13). The thickness of the laminar boundary layer grows but eventually a critical combination of properties (speed of flow, distance and viscosity) is exceeded after which the flow breaks down into the haphazard jumble of eddies characteristic of turbulent flow. However, note that a laminar sub-layer still remains at the surface. The thickness of the sub-layer mainly depends upon the roughness of the surface and the external wind speed. Over relatively smooth surfaces, and especially with high wind speeds, the layer becomes very thin or is temporarily absent.

In the laminar sub-layer there is no convection, therefore all non-radiative transfer is by molecular diffusion, and following equation 2.3 we can express the flux of heat through the layer as:

$$Q_H = -\rho c_p \kappa_{Ha} \frac{\partial \bar{T}}{\partial z} = -C_a \kappa_{Ha} \frac{\partial \bar{T}}{\partial z} \qquad (2.4a)$$

and for water vapour:

$$E = -\kappa_{Va} \frac{\partial \bar{\rho}_v}{\partial z} \qquad (2.4b)$$

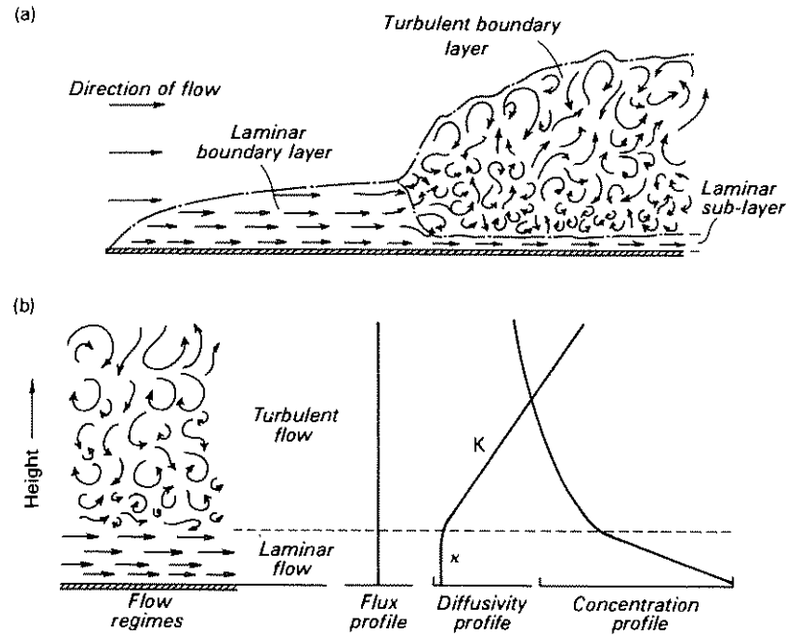

Figure 2.3 (a) Development of a laminar boundary layer over a flat plate and its transition to turbulent flow. (b) The vertical variation of the flux of any entity, the associated diffusion coefficients and the concentration of its property.

and for momentum:

$$\tau = \rho \kappa_{Ma} \frac{\partial \bar{u}}{\partial z} \qquad (2.4c)$$

where ρ – air density (kg m^{-3}), c_p – specific heat of air at constant pressure (J kg^{-1} K^{-1}), ρ_v – vapour density (p. 63), u – horizontal wind speed (m s^{-1}) and κ_{Ha}, κ_{Va} and κ_{Ma} are the molecular diffusion coefficient in air for the subscripted entities (m^2 s^{-1}). The values of these diffusivities are essentially constant depending only slightly on temperature (Appendix A3). κ values are very small, of the order of 10^{-5} m^2 s^{-1}, thus providing an important insulating barrier between the surface and the bulk of the atmosphere. Thus the gradients of climatic properties (T, ρ_v, u, etc.) are very steep in this layer, and since both the flux and the diffusivity are constant with height the vertical profile of a property is approximately linear, i.e. the gradient is constant.

In this book we will only concern ourselves with the laminar boundary layer when dealing with small objects, e.g. leaves or animals.

(iii) Roughness layer

Surface roughness elements cause complex flows around them including eddies and vortices. These three-dimensional effects are strongly dependent on the characteristics of the elements including their shape, plan density, flexibility, etc. Exchanges of heat, mass and momentum and the related climatic characteristics are difficult to express in this zone, but generalized features can be established.

(iv) Turbulent surface layer

There is no precise definition of this layer, but it is that part of the planetary boundary layer immediately above the surface where small-scale turbulence dominates transfer and vertical variation of the vertical fluxes is less than 10%. For this reason it is also referred to as the 'constant flux' layer. The depth of this layer is about 10% of the whole planetary layer. Turbulent diffusion is very much more efficient than that due to molecular activity, and the process is very different. Nevertheless meteorologists have found it useful to extend an analogy between the role played by eddies in convection to that of molecules in molecular diffusion. Hence using the flux-gradient formulation of equations 2.3 and 2.4, we will write closely analogous equations for heat mass and momentum transfer in the turbulent surface layer by merely replacing the κ's with K's called *eddy diffusivities* (see equations 2.9, 2.12, 2.14 and 2.17). These values are *not* simple constants, they vary greatly with time and space. In particular the K's vary with the size of the eddies and these increase with height above the surface (Figure 2.3). The value of the K's increases from about 10^{-5} m^2 s^{-1} near the top of the laminar sub-layer to as large as 10^2 m^2 s^{-1} well up into the planetary boundary layer. Given that the flux is essentially constant but that the diffusivity increases with height, we see that the profile of the related climatic property has a curved (usually logarithmic) shape with a decreasing gradient further away from the surface (Figure 2.3b).

The example of the air temperature profile in the lower portion of the turbulent surface layer is illustrated in Figure 2.2. By day temperatures decrease with height. This is referred to as a *lapse* profile. The gradient ($\partial T/\partial z$) has a negative sign[1] and the numerical rate of change with height is termed the lapse rate. At night temperature increases with height. This is called an *inversion* and the gradient has a positive sign. As in the soil case there is a lag for the surface temperature wave to penetrate up into the air due to the thermal inertia of the system, but it will be noted that the time is shorter in the air due to the greater diffusion by turbulence (see $T_{a1.2}$ in Figure 1.10b).

[1] This convention may not agree with some meteorology texts.

We noted in Section 1(b) that changes in climatic properties are due to flux convergence or divergence. Given the heat capacity of air (C_a) to be 1010 J m^{-3} K^{-1}, we find from equation 2.2 that a convergence of sensible heat (Q_H) of only 0·42 W m^{-2} in the lowest 1·2 m would be sufficient to explain the warming rates of about 1·25 K h^{-1} observed in the morning period of Figure 1.10b. Since such rates decrease with height (note the rapid decrease of the diurnal temperature range in Figure 2.2), they are consistent with the idea of a 'constant flux' layer to within 10% of the surface value.

Most of this book is concerned with conditions in the roughness and turbulent surface layers where interactions between the atmosphere and biosphere are concentrated.

(v) Outer layer

The turbulent region extending above the surface layer up to the top of the planetary boundary layer (i.e. 90% of its depth) is called the *outer layer*. Its depth is variable since it depends on the strength of turbulence generated at the ground surface. On a sunny day with light winds thermal convection may push the layer up to 1–2 km above the surface. At night with weak winds and little cloud it may contract to less than 100 m or become non-existent. On windy, cloudy days or nights the depth depends on the strength of the wind and the roughness of the surface. Defining the top of the layer is not always simple. It can be considered to be the depth of turbulent activity, which may not be easy to identify. Often it is set equal to the height of the lowest inversion. As will be shown, turbulence is damped by temperature inversions.

The effects of roughness in generating forced convection decrease more rapidly with height than the effects of heating on thermal convection. Therefore in the daytime most of the outer layer is dominated by free convection involving rather large eddy sizes associated with *thermals* (see p. 73) and heat plumes. They may even include organized convective circulation cells extending throughout its depth (Figure 2.4a). This may lead to small cumulus clouds at the topmost limb of the updrafts. Often the mixing of airborne materials (e.g. dust, pollutants, spores, etc.) is so efficient that the whole of the layer is occupied by a uniform haze. Hence the daytime convective layer is called the *mixed layer*.

In this excellent mixing layer profiles of climatic properties show very little variation with height as illustrated by the daytime temperature profile in Figure 2.4a. The flux profile usually shows an approximately linear decrease with height, becoming zero near the inversion base. In the case of heat (Q_H) the flux actually reverses direction in the topmost 10% of the mixed layer (Figure 2.4a). This is due to the turbulent activity which causes thermals to bombard the base of the inversion. Some overshoot into

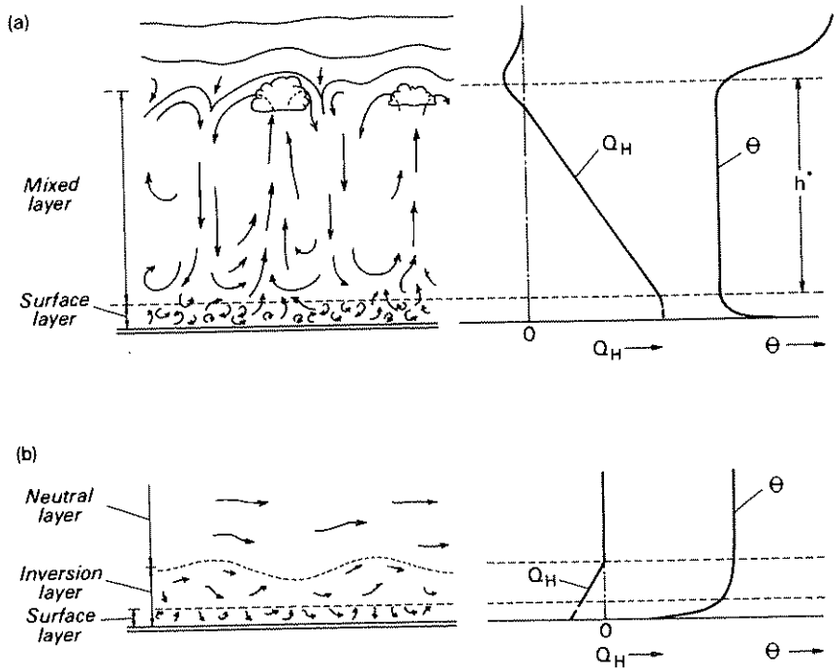

Figure 2.4 Schematic representation of airflows in the outer layer. (a) The daytime mixed layer, and the associated vertical profiles of the sensible heat flux density (Q_H) and potential temperature (θ) within a mixed layer of depth h^*. (b) The corresponding conditions in the nocturnal stable layer. (Note – see p. 53 for the definition of θ.)

the overlying warmer air and when they are repelled they transport heat downwards. This is referred to as *convective entrainment.*

At night, due to stability, turbulence is largely restricted to a shallow layer. Convection is entirely of mechanical origin. A true mixed layer is not present, but turbulent transfer removes heat from the lowest layer to form an inversion layer (Figure 2.4b). Turbulenc may even become so weak that radiative flux divergence plays a role in shaping the temperature profile. At the top of the inversion layer turbulence may break down into wave-like oscillations.

2 SUB-SURFACE CLIMATES

(a) Soil heat flux (Q_G) and soil temperature (T_s)

Heat transfer and the thermal climate of soils are governed by four linked thermal properties: thermal conductivity, heat capacity, thermal diffusivity

and thermal admittance. As already noted, heat is conducted down into the soil by day and upwards at night. We can re-write equation 2.3 to express this sensible heat flux density (Q_G) as Fourier's law:

$$Q_G = -k_s \frac{\partial \overline{T}_s}{\partial z} \simeq -k_s \frac{(\overline{T}_2 - \overline{T}_1)}{(z_2 - z_1)} \qquad (2.5)$$

where the subscripts refer to levels in the soil (see Figure 2.2). As before, the sign indicates the flux is in the direction of decreasing temperature, therefore by day when $\partial \overline{T}_s/\partial z$ is negative the equation gives a positive value of Q_G which is in accord with the flux convention adopted on p. 23; k_s is known as the *thermal conductivity* (W m^{-1} K^{-1}), which is a measure of the ability to conduct heat. It is formally defined as the quantity of heat (J) flowing through unit cross-sectional area (m^2) of the substance in unit time (s), if perpendicular to it there exists a temperature gradient of 1 degree m^{-1}. Typical values for a range of natural materials are listed in Table 2.1; of these motionless air is the most notable because it is such a very poor conductor of heat (i.e. it is a good insulator).

Unfortunately k_s is not a simple constant for a given soil. It varies both with depth and with time. However if we restrict ourselves to bulk averages k_s depends upon the conductivity of the soil particles, the soil porosity, and the soil moisture content. Of these the soil moisture content is the only short-term variable for a given soil. The addition of moisture to an initially dry soil increases its conductivity (Figure 2.5a). This happens for two reasons. First, coating the soil particles increases the thermal contact between grains. Second, since the soil pore space is finite the addition of pore water must expel a similar amount of pore air. From Table 2.1 we can see that this means replacing soil air with a substance whose conductivity is more than an order of magnitude greater.

We have already introduced heat capacity (C) (p. 36). It relates to the ability of a substance to store heat and expresses the temperature change produced as a result of gaining or losing heat. The value of C_s for a soil can be calculated by evaluating the fractions of soil solid, water and air (Appendix A2, p. 375). The value for a given soil is strongly dependent, in an almost linear fashion, on the soil moisture content (Figure 2.5b). Adding water with a very high heat capacity excludes a proportionate volume of soil air of low heat capacity (see Table 2.1). The result is a reduction in the soil's thermal sensitivity.

The thermal diffusivity of a soil (κ_{Hs}) is its ability to diffuse thermal influences. It controls the speed at which temperature waves move and the depth of thermal influence of the active surface. From equations 2.3 and 2.5 we see that $\kappa_{Hs} = k_s/C_s$ which shows that thermal influences are directly proportional to the ability to conduct heat (k_s) but inversely proportional to the amount of heat necessary to effect temperature change (C_s). Thermal diffusivity may be viewed as a measure of the time required

Table 2.1 Thermal properties of natural materials

Material	Remarks	ρ Density (kg m^{-3} × 10^3)	c Specific heat (J kg^{-1} K^{-1} × 10^3)	C Heat capacity (J m^{-3} K^{-1} × 10^6)	k Thermal conductivity (W m^{-1} K^{-1})	κ Thermal diffusivity (m^2 s^{-1} × 10^{-6})	μ Thermal admittance (J m^{-2} s$^{-1/2}$ K^{-1})
Sandy soil	Dry	1·60	0·80	1·28	0·30	0·24	620
(40% pore space)	Saturated	2·00	1·48	2·96	2·20	0·74	2550
Clay soil	Dry	1·60	0·89	1·42	0·25	0·18	600
(40% pore space)	Saturated	2·00	1·55	3·10	1·58	0·51	2210
Peat soil	Dry	0·30	1·92	0·58	0·06	0·10	190
(80% pore space)	Saturated	1·10	3·65	4·02	0·50	0·12	1420
Snow	Fresh	0·10	2·09	0·21	0·08	0·10	130
	Old	0·48	2·09	0·84	0·42	0·40	595
Ice	0°C, pure	0·92	2·10	1·93	2·24	1·16	2080
Water*	4°C, still	1·00	4·18	4·18	0·57	0·14	1545
Air*	10°C, still	0·0012	1·01	0·0012	0·025	21·50	5
	Turbulent	0·0012	1·01	0·0012	~125	~10 × 10^6	390

* Properties depend on temperature, see Appendix A3.
Sources: van Wijk and de Vries (1963), List (1966).

Figure 2.5 Relationship between soil moisture content: (a) thermal conductivity, (b) heat capacity, (c) thermal diffusivity and (d) thermal admittance for most soils.

for temperature changes to travel. For example, the daytime heat input will generate a temperature wave that travels rapidly and to considerable depth in soil where conductivity is high, but if it takes large amounts of heat to warm intermediate layers because of a high heat capacity it will be slowed and not penetrate as far. Typical values of κ_{Hs} are given in Table 2.1.

The value of κ_{Hs} is obviously affected by the same soil properties that influence k_s and C_s, especially soil moisture (Figure 2.5c). Note that adding moisture to a dry soil initially produces a sharp increase in κ_{Hs} by increasing thermal contact and expelling soil air (i.e. increasing k_s as in Figure 2.5a). However, in most soils beyond about 20% soil moisture content by volume κ_{Hs} begins to decline. This happens because whereas k_s levels off (Figure 2.5a) the value of C_s continues to increase at higher moisture contents (Figure 2.5b).

Soils with high diffusivities allow rapid penetration of surface temperature changes and permit these effects to involve a thick layer. Thus for the same heat input their temperature regimes are less extreme than for soils with low diffusivities. By day the surface heating is used to warm a thick layer of soil, and at night the surface cooling can be partially offset by drawing upon heat from a similarly thick stratum. Soils with poor diffusi-

vities concentrate their thermal exchanges only in the uppermost layer, and consequently experience relatively extreme diurnal temperature fluctuations. Therefore, in general a wet clay has a conservative thermal climate, whereas an almost dry peat is extreme.

This is a convenient juncture to introduce a related thermal property called the soil *thermal admittance* ($\mu_s = C_s\kappa_{Hs}^{1/2} = (k_sC_s)^{1/2}$. Technically this is a *surface* rather than a soil property. It is a measure of the ability of a surface to accept or release heat since it expresses the temperature change produced by a given heat flux change. This is why some materials with high μ (such as metals) initially feel cooler to the touch than those with low μ (such as wood) even though both are actually at the *same* room temperature of, say, 20°C (for values see Table 7.4). Your finger is at a temperature of about 30°C and the 10-degree temperature difference is rapidly sensed at a surface of high μ because heat transfer at the finger-material interface is excellent. Similarly, note the *apparent* difference of placing your bare foot on a clay tile bathroom floor compared with a bathmat or cork tile. On the other hand, if the materials being touched are at a higher temperature than your hand or foot, that with higher μ would initially feel warmer.

A surface also has an analogous atmospheric admittance ($\mu_a = C_aK_H^{1/2}$). The relative magnitude of the two properties are important in determining the sharing of sensible heat between the soil and the atmosphere since:

$$\mu_s/\mu_a = Q_G/Q_H$$

The amplitude of the surface temperature wave is closely linked to these properties. The larger these values are the easier it is for heat to be transported to or from the interface and the smaller will be the surface temperature variations. For a given site the value of μ_a is determined by the state of turbulence (i.e. the eddy diffusivity, K_H), and μ_s by the soil moisture (Figure 2.5d). For a given state of the atmosphere, sites with large μ_s (Table 2.1) will accept or release heat to or from soil storage with relative ease and hence will exhibit relatively small surface temperature changes through a day.

The course of soil temperature with time is very regular in comparison with any other atmospheric element. Typical soil temperature variations at a number of depths on a cloudless day are given in Figure 2.6a. The near-surface temperature variation is wave-like and agrees closely with that of the surface. The wave penetrates downward to lower depths, but in doing so its amplitude decreases, and the times of maximum and minimum temperature are lagged (shift to the right in time). Both features depend on κ_s. The wave amplitude at any depth $(\Delta\overline{T}_s)_z$ is given by:

$$(\Delta\overline{T}_s)_z = (\Delta\overline{T})_0 e^{-z(\pi/\kappa_{Hs}P)^{1/2}} \qquad (2.6)$$

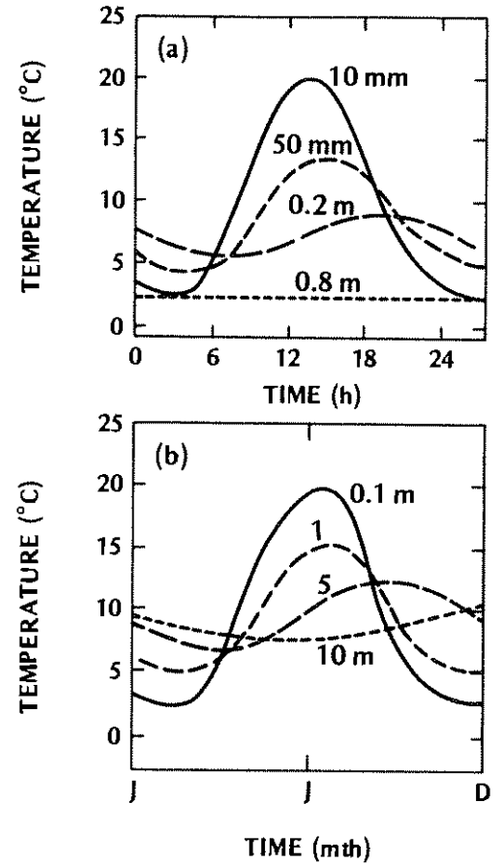

Figure 2.6 Generalized cycles of soil temperature at different depths for (a) daily and (b) annual periods.

where, $(\Delta\overline{T})_0$ – surface temperature wave amplitude, e – base of Naperian logarithms, P – wave period (s). This shows that the diurnal temperature range decreases exponentially with depth. In most soils the daily surface temperature wave is only discernible to a depth of about 0·75 m. In soils with low κ_s values it is even less, indicating that flux convergence has extinguished Q_G in a thin near-surface layer. The time lag for the wave crest (maximum) and trough (minimum) to reach lower depths is given by:

$$(t_2 - t_1) = \frac{(z_2 - z_1)}{2}(P/\pi\kappa_{Hs})^{1/2} \qquad (2.7)$$

where t_1 and t_2 are the times at which the wave crest or trough reaches depths z_1 and z_2. Note that because of this time lag, at any given time the

soil may be cooling in its upper layers but warming at only a short distance beneath, and vice versa when the upper layers are warming (Figure 2.6a).

The annual soil temperature regime (Figure 2.6b) follows a wavelike pattern entirely analogous with the diurnal one. The wave period is of course dependent upon the annual rather than the daily solar cycle. With that adjustment, equations 2.6 and 2.7 still apply to the wave amplitude and lag with depth. With a longer period the wave amplitude decreases less rapidly with depth, and the depth of the affected layer is much greater than for the diurnal case. In fact the difference between the depth of penetration of the annual and daily waves is approximated by the square root of the ratio of their respective periods, i.e. $(3{\cdot}15 \times 10^7 s / 8{\cdot}64 \times 10^4 s)^{1/2} \simeq 19$. Therefore given the daily depth is 0.75 m in typical soils, the annual wave may penetrate to about 14 m. This would then be termed the depth of zero annual range. The temperature at this depth is sometimes used as a surrogate for the average annual air temperature of the site. This is based on the premise that long-term thermal equilibrium exists between the soil and the atmosphere. During the warm season soil temperatures decrease with depth and the associated downward heat flux builds up the soil's heat store. In the cold season the gradient is reversed and the store is gradually depleted. The spring and autumn are transitional periods when the soil temperature gradient reverses sign. These reversals (or 'turnovers') are important biological triggers to soil animals and insects. In the spring they may come out of hibernation, and/or move upwards towards the warmer surface layers. In the autumn they retreat to depths where soil warmth is more equable.

The effects of cloud on the diurnal soil temperature pattern are fairly obvious. With overcast skies absolute temperatures are lower by day but warmer at night, and the wave amplitude is smaller; variable cloudiness induces an irregular pattern upon the diurnal wave. Using the same argument as for the annual/daily comparison a 15 min temperature variation induced by cloud would only travel about one tenth of the distance of the daily wave, so typically it would not be registered below about 75 mm. Rainfall is capable of either increasing or decreasing soil temperatures depending upon the temperature of the rain in comparison with the soil. It is also capable of transporting heat as it percolates down through the soil. The effects of a snow or vegetation cover over the soil are dealt with in Chapters 3 and 4, respectively.

Appendix A2 (pp. 359 and 374) provides examples of the instruments for measuring soil heat flux and soil temperature in the field.

(b) Soil water flow (J) and soil moisture (S)

Soil moisture is usually expressed in one of two ways. *Soil moisture content* (*S*) is a measure of the actual water content, and is defined as the

percentage volume of a moist soil occupied by water. This is particularly pertinent in water balance studies (p. 31) where changes in mass are important. *Soil moisture potential* (Ψ) on the other hand is an indirect measure of water content, and may be visualized as the energy necessary to extract water from the soil matrix. The units of Ψ are those of negative pressure (Pa = mb $\times 10^{-2}$), which can also be expressed as a head of water displaced (1 m head of water = $1{\cdot}0 \times 10^4$ Pa). This concept is of value in estimating the availability of water for plant use, and in calculating moisture movement. Methods for determining these two terms are given in Appendix A2 (p. 388).

The forces which bind soil water are related to the soil porosity and the soil water content (Figure 2.7). The forces are weakest in the case of open textured, wet soils, and greatest for compact dry soils. Thus at a given value of *S* the water potential is greatest for a clay, least for a coarse sand, and intermediate for a loam. Similarly in a given soil the potential increases as *S* decreases, but not in a linear fashion. It is relatively easy to extract moisture from a wet soil but as it dries out it becomes increasingly difficult to remove additional units. Figure 2.7 shows that in the range of water potentials which permit plants to extract soil water, sand has the least available water (7% vol.) and a silt loam the most (16% vol.).

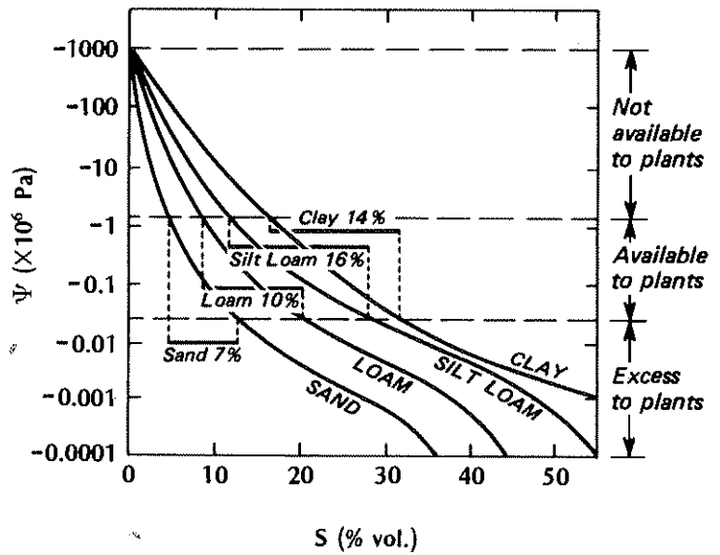

Figure 2.7 Relationship between soil moisture potential (Ψ) and soil moisture content (*S*) in soils with different textures. Heavy horizontal bars show the volumetric water available to plants (modified after Buckman and Brady. 1960).

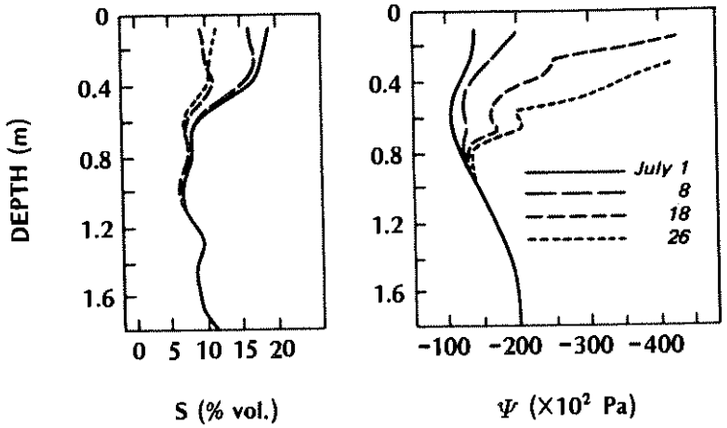

Figure 2.8 Profiles of soil moisture content (S) and soil moisture potential (Ψ) in a sandy loam during a drying phase (after Rouse and Wilson, 1972).

Figure 2.8 conveniently illustrates these two concepts of soil moisture. It shows profiles of both S and Ψ at the same site during a period of one month when the soil was almost continually drying-out. As S decreased throughout the period, the value of Ψ increased. It is possible to utilize such changes in soil moisture content to estimate evapotranspiration losses to the atmosphere by integrating the area between successive profiles in time. In this case it appears as though the soil down to a depth of 0·8 m participated in the soil-air exchange.

The vertical flux of soil water (J) in the absence of percolating rain, is composed of both liquid (J_l) and vapour (J_v) flow. The movement of liquid moisture in a saturated or unsaturated soil may be considered analogous with the flux-gradient relationship for heat (equation 2.3). In this case the flux of water is related to the vertical water potential gradient by Darcy's Law:

$$J_l = -K_f \frac{\partial \bar{\Psi}}{\partial z} \qquad (2.8)$$

where K_f – hydraulic conductivity. The effect of evapotranspiration is to create a potential gradient which becomes greater than the opposing gravitational gradient and encourages the upward movement of water from low to high water potential. Unfortunately in unsaturated soils K_f is not a constant, but depends on both S and Ψ as well as other soil factors.

The flow of water vapour (J_v) obeys the flux-gradient relationship of equation 2.4b:

$$J_v = -\kappa_{Va} \frac{\partial \bar{\rho}_v}{\partial z}$$

where κ_{Va} – molecular diffusivity for water vapour (see Appendix A3, p. 393) and ρ_v – vapour density (p. 63) or water vapour concentration. The air in the pore spaces of moist soils is in close contact with soil water and is therefore commonly close to being saturated. The saturation vapour concentration is directly related to temperature (see Figure 2.15), being higher at higher temperatures. This creates a water vapour concentration gradient and a corresponding vapour flux from high to low soil temperatures. Thus noting the temperature distributions in Figures 2.2 and 2.6a, there is a tendency for vapour to flow down into the soil by day and up towards the surface at night. The nocturnal vapour flux in the soil commonly results in condensation upon the cold soil surface known as *distillation*. This is not the same process as dewfall (p. 67) which involves the turbulent transfer of atmospheric vapour down onto the surface.

3. SURFACE LAYER CLIMATES

(a) Lapse rates and stability

The dominant process in the lower atmosphere is convection (free, forced and mixed, see p. 16). A major control on the type and extent of convective activity is the vertical temperature structure as expressed in the concept of stability. Therefore it is helpful to explain stability before proceeding.

Consider a discrete parcel of air moving up through the atmosphere, and assume that it neither receives nor gives out heat to the surrounding air (such a parcel is said to be moving *adiabatically*). As it rises it encounters lower atmospheric pressure because the mass of air above it becomes progressively less. Thus the internal pressure of the parcel becomes greater relative to its surroundings and the parcel will tend to expand. To push away the surrounding air requires work and therefore energy. But the only energy available is the thermal energy of the parcel itself (since we are assuming no exchange with the surroundings), thus as the parcel rises it cools. In dry (unsaturated) air the rate of temperature change of such a parcel with height is the constant value of $9{\cdot}8 \times 10^{-3}$°C m^{-1} called the *dry adiabatic lapse rate* (Γ). If the parcel becomes saturated some vapour condenses into droplets thereby releasing latent heat (L_v) which reduces the rate of cooling, but the value is not constant. In most of the applications in this book (i.e. in the boundary layer below cloud base height) the dry adiabatic assumptions are approximately valid. Eventually of course the parcel will cease to rise and will impart its heat by mixing with the air at that level.

It is important however not to confuse the dry adiabatic lapse rate (Γ) with the *environmental lapse rate* (ELR). The former is the rate at which a dry parcel will cool if it is moved upward through the atmosphere, and

also the rate at which it will warm if it moves down towards the ground (i.e. when it encounters increased atmospheric pressure and becomes compressed). The ELR, on the other hand, is a measure of the actual temperature structure existing above a given location as sensed by thermometers at fixed heights on a mast, or attached to a balloon or an aircraft. The temperature structure above a location is quite likely to exhibit variations in the ELR in different layers, some being lapse, some inversion and some isothermal.

Atmospheric stability may be viewed as the relative tendency for an air parcel to move vertically. It can be evaluated in a dry atmosphere by comparing the values of the actual ELR at any time against the constant rate Γ, in the following manner. First, select the level of interest, z_1. In microclimatological applications we are usually interested in the stability of air near the ground, but in the examples which follow we will choose some other level so that we can illustrate the results of both upward and downward displacement. Secondly, construct a line with slope Γ (such a line is called a dry *adiabat*) so as to intersect the ELR at the selected level, z_1. From the preceding discussion we know that any parcel displaced above (below) that level will cool (warm) according to Γ (i.e. its temperature will follow the adiabat). Third, when the displacing force is removed at any level the future motion of the parcel depends on its density relative to the environmental air at the same level, so we compare the two temperatures. If the parcel is warmer than the air around, it will be less dense, possess *buoyancy*, and continue to rise unaided rather like the heated water at the bottom of a kettle. Conversely, if it is colder, and therefore denser than its surroundings, it will sink. If the air in the parcel and surrounding environment at the same level are identical, the parcel possesses no net buoyancy and will remain static.

Three possibilities exist depending upon the value of the ELR, namely:

(i) ELR greater than Γ – this is the situation described by ELR_1 in Figure 2.9a and is typical of sunny days near the ground when surface heating gives rise to a strong lapse rate. If a parcel at z_1 is displaced upwards its temperature (which follows Γ) is always higher than that of the environmental air, therefore if the displacing force is removed it possesses buoyancy and will continue to rise. The layer is therefore said to be *unstable*. The greater the value of ELR_1 the greater is the divergence between the two lines and hence the greater the instability. Notice also that had the parcel originally been displaced below z_1 it would always find itself colder than the environmental air, and if left alone would tend to continue sinking. Instability is therefore independent of the direction of displacement.

(ii) ELR smaller than Γ – if the ELR is negative or between 0 and $9{\cdot}8 \times 10^{-3}$°C m^{-1} the layer is *stable*. These conditions are obviously

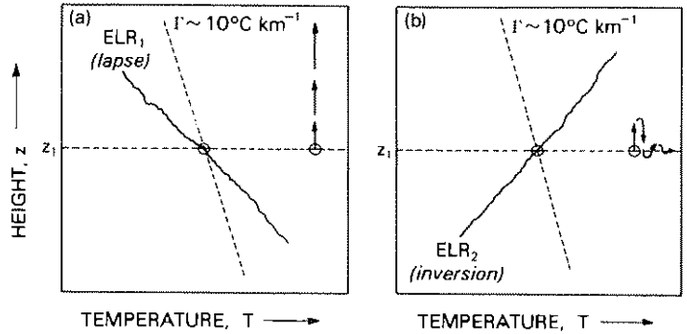

Figure 2.9 Height vs temperature graphs illustrating (a) unstable and (b) stable atmosphere. The uneven line is measured temperature profile (ELR), and the broken, sloping line is a dry adiabat drawn through level z_1 (for details see text). Arrows at right give visual impression of motion of a parcel displaced above z_1. Motion would be a mirror image if displacement were downward.

met in an inversion such as that described by ELR_2 in Figure 2.9b. In this case a displaced parcel above z_1 always finds itself colder than the environmental air and hence tends to sink back towards z_1. Equally if displaced below z_1 it would find itself warmer and tend to rise back up to its equilibrium position. The greater the difference between the ELR and Γ the greater is the damping tendency.

(iii) ELR equal to Γ – in this situation (not shown in Figure 2.9) the layer is said to be *neutral*. After displacement to any level above or below its initial position z_1, the temperature of the parcel and of the air are the same. Hence there will be no relative tendency for the parcel to rise or sink, and if the displacing force is removed the parcel remains stationary. This situation occurs in the boundary layer under cloudy, windy conditions. Cloud restricts surface heating and cooling thereby minimizing the development of any horizontal temperature stratification, and wind helps to homogenize the temperature structure by vigorous mechanical convection.

When considering atmospheric stability it is often useful to use *potential temperature* (θ) instead of the observed air temperature (T). We have seen that the temperature of parcels behaving adiabatically is related to pressure. In order to compare parcels existing at different pressures (levels in the atmosphere) it is therefore useful to standardize conditions to a common pressure. The potential temperature of a parcel is the value it would have if it were at the arbitrary pressure value of 100 kPa. This is tantamount to correcting the observed temperature to allow for Γ, so that

replotting Figure 2.9 using θ involves rotating all environmental profiles clockwise by the slope of Γ. Interpretation of stability now becomes straightforward. If the ELR plotted as θ is constant with height (i.e. a vertical line, $\partial\theta/\partial z = 0$) the layer is neutral; if the ELR slopes to the left it is unstable, and to the right it is stable.

Examples of vertical temperature profiles plotted using *both* θ and T are given in Figure 2.14 (see p. 62). It also shows that with fine weather it is normal for the planetary boundary layer to be unstable by day and stable by night. Exceptions occur over high latitude snow surfaces in winter where the boundary layer is stable for long periods, and over tropical ocean surfaces where it may be unstable for equally long spells.

It is also important to realize that the atmosphere is commonly made up of a number of layers of different stability. For example, the daytime convective boundary layer shown in Figure 2.4a consists of an unstable surface layer ($\partial\theta/\partial z < 0$) and an almost neutral mixed layer ($\partial\theta/\partial z \simeq 0$) and is capped by an elevated inversion layer ($\partial\theta/\partial z > 0$). This stable capping layer, which is almost impenetrable to air parcels rising from below, is extremely important because it effectively traps the heat, water vapour and pollutants (released at the surface) within the boundary layer. Examples of stability changes due to a variety of atmospheric processes are given in Chapter 9.

(b) Momentum flux (τ) and wind (u)

The wind field in the boundary layer is largely controlled by the frictional drag imposed on the flow by the underlying rigid surface. The drag retards motion close to the ground and gives rise to a sharp decrease of mean horizontal wind speed ($\bar{u}$) as the surface is approached (Figure 2.10). In the absence of strong thermal effects the depth of this frictional influence depends on the roughness of the surface (Figure 2.10a). The profiles in this figure are based on measurements in strong winds, and the height z_g is the top of the boundary layer above which $\bar{u}$ is approximately constant with height (i.e. surface drag is negligible). The depth of this layer increases with increasing roughness. Therefore the vertical gradient of mean wind speed ($\partial\bar{u}/\partial z$) is greatest over smooth terrain, and least over rough surfaces. In light winds the depth z_g also depends upon the amount of thermal convection generated at the surface. With strong surface heating z_g is greater than in Figure 2.10a, and with surface cooling it is less (see also p. 71).

The force exerted on the surface by the air being dragged over it is called the *surface shearing stress* (τ) and is expressed as a pressure (Pa, force per unit surface area). This force is equally opposed by that exerted by the surface on the atmosphere. However since air is a fluid it only acts on the lower boundary and not throughout the total bulk of the atmosphere. The

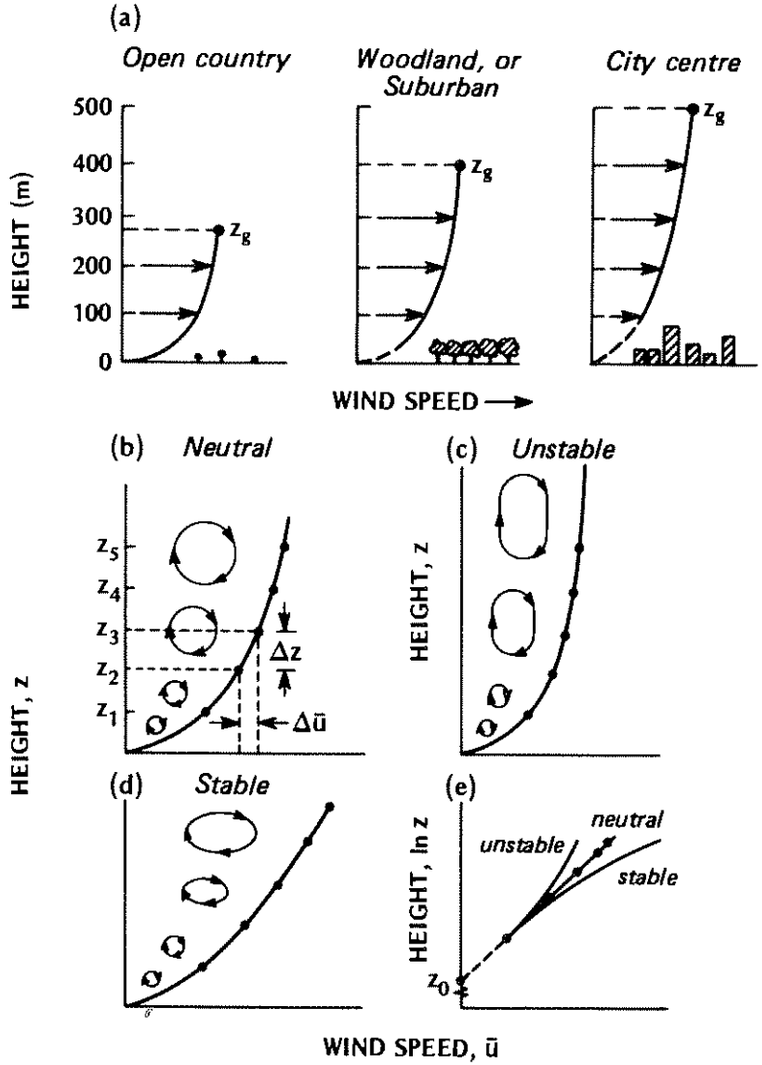

Figure 2.10 The wind speed profile near the ground including: (a) the effect of terrain roughness (after Davenport, 1965), and (b) to (e) the effect of stability on the profile shape and eddy structure (after Thom, 1975). In (e) the profiles of (b) to (d) are re-plotted with a natural logarithm height scale.

surface layer of frictional influence generates this shearing force and transmits it downwards as a *flux of momentum*. In the 'constant-flux' layer τ does not vary by more than 10% and hence atmospheric values are approximately equal to those at the surface.

The flux of momentum is not as easy to visualize as that of heat or water vapour, but the following simple conceptualization may help. The momentum possessed by a body is given by the product of its mass and velocity. In the case of air the mean horizontal momentum of unit volume is therefore given by its density (ρ) multiplied by its mean horizontal wind speed (i.e., momentum = $\rho\bar{u}$). Since for practical purposes we may consider air density to be constant in the surface layer (see Appendix A3, p. 393) the mean horizontal momentum possessed by different levels is proportional to the profile of wind speed (i.e., it increases with height).

Consider the situation at level z_3 in Figure 2.10b. Due to the effects of forced convection generated by the surface roughness, and the mutual shearing between air layers moving at different speeds, turbulent eddies are continually moving up and down through z_3. An eddy arriving at z_3 having originated at z_4 above will, upon mixing, impart a net increase in velocity (and hence momentum). A fast-response wind speed sensor at z_3 would therefore see this downdraft as an increase in wind speed, or a 'gust'. Conversely an updraft from z_2 would be sensed as a 'lull' in horizontal wind speed. Notice that due to the increase of wind with height the net effect of *both* updrafts and downdrafts is always to sustain a net flux of momentum downwards. In the turbulent surface layer this vertical flux of horizontal momentum is given:

$$\tau = \rho K_M \frac{\partial \bar{u}}{\partial z} \tag{2.9}$$

where K_M – eddy viscosity ($m^2\ s^{-1}$). Equation 2.9 is an example of the way the molecular analogy is extended to turbulent flow (p. 40). It relates the flux (τ) to the gradient of horizontal momentum ($\rho \cdot \partial\bar{u}/\partial z$) and the ability of the eddies to transfer momentum (K_M).

In terms of the general characteristics of the interaction between different surfaces and airflow we may expect that for a surface of given roughness τ will depend upon $\bar{u}$. As $\bar{u}$ at a reference level increases so will τ, and so will the depth of the forced convection layer. Similarly if we considered the value of $\bar{u}$ to be constant over surfaces with different roughnesses, the magnitude and depth of forced convective activity would be greatest over the roughest surface (Figure 2.10a).

The actual form of the wind variation with height under neutral stability (p. 53) has been found to be accurately described by a logarithmic decay curve. Thus using the natural logarithm of height (ln z) as the vertical co-ordinate the data from Figure 2.10b fall upon a straight line in Figure 2.10e. This provides the basis for the logarithmic wind profile equation:

$$\bar{u}_z = \frac{u_*}{k} \ln \frac{z}{z_0} \tag{2.10}$$

where $\bar{u}_z$ – mean wind speed ($m\ s^{-1}$) at the height z, u_* – *friction velocity* ($m\ s^{-1}$), k – von Karman's constant ($\simeq 0{\cdot}40$), z_0 – *roughness length* (m). It has been found that the shearing stress is proportional to the square of the wind velocity at some arbitrary reference height. Thus we introduce u_* for which this square law holds exactly so that:

$$u_*^2 = \tau/\rho \tag{2.11}$$

This is helpful because u_* can be evaluated from wind profile measurements (the slope of the line in Figure 2.10 is k/u_*) and therefore we can obtain τ, which can be used in evaluating other fluxes (Appendix A2).

The length z_0 is a measure of the aerodynamic roughness of the surface. It is related, but not equal to, the height of the roughness elements. It is also a function of the shape and density distribution of the elements. Typical values of z_0 are listed in Table 2.2. This term is defined as the height at which the neutral wind profile extrapolates to a zero wind speed (Figure 2.10e). An alternative means of evaluation is given on p. 139.

The foregoing discussion relates to neutral conditions where buoyancy is unimportant. Such conditions are found with cloudy skies and strong winds, and in the lowest 1 to 2 m of the atmosphere. Cloud reduces radiative heating and cooling of the surface; strong winds promote mixing and do not permit strong temperature stratification to develop; and in the lowest layers forced convection due to frictionally-generated eddies is dominant. In the simplest interpretation these eddies may be conceived as

Table 2.2 Aerodynamic properties of natural surfaces

Surface	Remarks	z_0 Roughness length (m)	d Zero plane displacement* (m)
Water†	Still – open sea	$0{\cdot}1-10{\cdot}0 \times 10^{-5}$	–
Ice	Smooth	$0{\cdot}1 \times 10^{-4}$	–
Snow		$0{\cdot}5-10{\cdot}0 \times 10^{-4}$	–
Sand, desert		0·0003	–
Soils		0·001–0·01	–
Grass†	0·02–0·1 m	0·003–0·01	≤ 0·07
	0·25–1·0 m	0·04–0·10	≤ 0·66
Agricultural crops†		0·04–0·20	≤ 3·0
Orchards†		0·5–1·0	≤ 4·0
Forests†	Deciduous	1·0–6·0	≤ 20·0
	Coniferous	1·0–6·0	≤ 30·0

* Only approximate, calculated as $d \simeq \frac{2}{3}h$ (see p. 116)
† z_0 depends on wind speed (see p.139)
Sources: Sutton (1953), Szeicz *et al.* (1969), Kraus (1972).

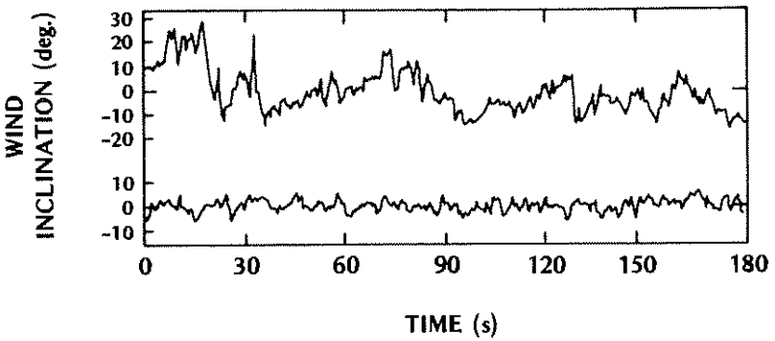

Figure 2.11 The effect of stability on the turbulent structure of the atmosphere. Wind inclination fluctuations at a height of 29 m during unstable (upper trace) and stable (lower) conditions over a grass site with winds of 3 to 4 m s^{-1} (after Priestley, 1959).

being circular and to increase in diameter with height (Figure 2.10b). In reality they are three-dimensional and comprise a wide variety of sizes.

In unstable conditions the vertical movement of eddies (and therefore the momentum flux) is enhanced. Near the surface mechanical effects continue to dominate but at greater heights thermal effects become increasingly more important. This results in a progressive vertical stretching of the eddies and a reduction of the wind gradient (Figure 2.10c). Conversely strong stability dampens vertical movement, progressively compresses the eddies and steepens the wind gradient (Figure 2.10d).

Stability effects on turbulence are further illustrated in Figure 2.11. This is a graph of wind inclination (roughly corresponding to vertical winds, because the scale refers to the tilt angle of a horizontal vane) over a period of 3 minutes. The upper trace is from lapse (unstable), and the lower trace from inversion (stable) conditions, over the same grass site with approximately equivalent horizontal wind speeds. Thus differences between the two traces are due to stability differences. In the unstable case two types of fluctuation are evident. First, there are long-period 'waves' lasting about 1 to 1·5 minutes. These are relatively large buoyancy-generated eddies bursting up through the measurement level (positive values) or being replaced by sinking air parcels (negative values). Superimposed on this pattern are a second set of much shorter-period fluctuations. These are the small roughness-generated and internal shearing eddies. Therefore Figure 2.11 visually presents the two elements of turbulence – free convection (large) and forced convection (small). The combination of these two elements (upper trace) provides a very efficient means of both vertical transport and mixing. This is the 'ideal' daytime mixed convection situation. The stable case (lower trace) by contrast only exhibits the short-period eddies due to

forced convection because buoyancy is absent. This is the 'ideal' nocturnal situation, and is not conducive to vertical exchange.

In summary we may say that below approximately 2 m the effects of forced convection dominate even in non-neutral conditions as long as there is a reasonable airflow. Above this height the relative role of free convection grows and the possibility of stability effects on momentum transfer increases. These effects are manifested as curvature in the wind profile (Figure 2.10b–e). Strong instability weakens the wind gradient by promoting vertical exchange over a deep layer, and thereby mixing the greater momentum of faster-moving upper air with that nearer the surface. Strong stability on the other hand strengthens the wind gradient. It therefore follows that since there is a characteristic diurnal cycle of stability there is an associated diurnal variation of wind speed in the surface layer (see p. 75).

The study of momentum exchange and the form of the wind profile is important because of what it tells us about the state of turbulence. This is central to questions concerning the transport of heat and water vapour and to the dispersal of air pollutants.

(c) Sensible heat flux (Q_H) and air temperature (T_a)

In the turbulent surface layer the flux of sensible heat is given by:

$$Q_H = -C_a K_H \left(\frac{\partial \overline{T}}{\partial z} + \Gamma \right) = -C_a K_H \left(\frac{\partial \overline{\theta}}{\partial z} \right) \qquad (2.12)$$

where, K_H – eddy conductivity (m^2 s^{-1}). The form of equation 2.12 is directly analogous to that of equation 2.9 for momentum transfer, and the value of K_H is similar to that of K_M. The direction of the heat transfer (sign of Q_H) is determined by the sign of the temperature gradient. By day the gradient is negative (lapse) and Q_H is positive (i.e. directed from the surface into the lower atmosphere). By night the gradient is positive (inversion) and Q_H is negative. The term Γ is included to correct the observed temperature gradient for the effects of vertical atmospheric pressure changes. It is only of importance if the height interval is large (e.g. greater than 2 m). The use of potential temperature (θ) incorporates these effects (p. 53).

The vertical transfer of sensible heat by eddies can be visualized with the aid of Figure 2.12. This shows the variation of air temperature (T), vertical velocity (w) and the associated instantaneous flux of heat over a period of 120 s from fast-response instruments placed at a height of 23 m over a grass surface at Edithvale, Australia. The data are from a daytime unstable period, and the vertical wind velocity pattern clearly resembles the upper trace of Figure 2.11. The simultaneous record of air temperature exhibits

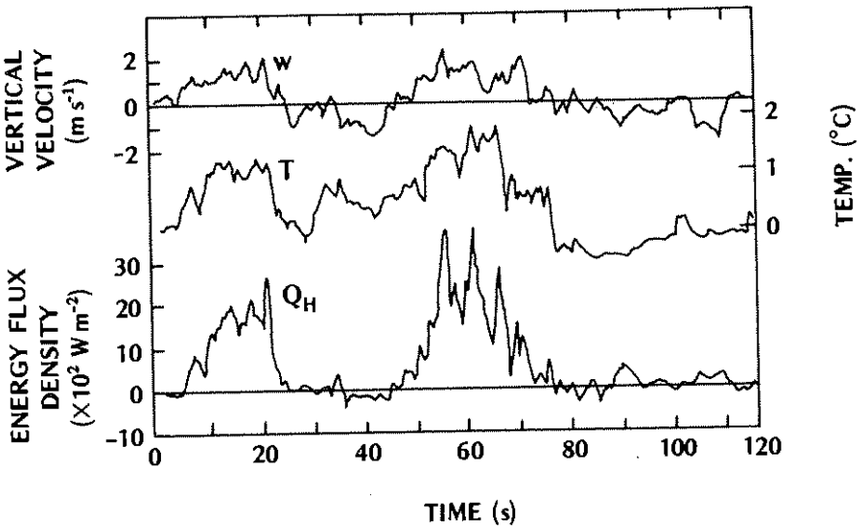

Figure 2.12 The relationships between vertical velocity (w) and air temperature (T) fluctuations, and the instantaneous sensible heat flux (Q_H). Results from fast-response instruments at a height of 23 m over grass in unstable conditions (after Priestley, 1959).

the same pattern, and moreover its fluctuations are closely in phase with those of the vertical wind. Thus in unstable conditions an updraft (positive w) is associated with an increase of T, and downdraft (negative w) with a decrease of T, relative to its mean value. This occurs because unstable conditions are associated with a lapse T profile, and an updraft through the measurement level has originated closer to the ground where it is warmer. Conversely a downdraft comes from higher levels where it is cooler. For both situations (up- and downdraft) the net sensible heat transfer is therefore upwards. The instantaneous heat flux (lowest trace in Figure 2.12) also shows that most of the transfer tends to occur in 'bursts' coinciding with the upward movement of a buoyant thermal (p. 73). Closer to the surface this pattern is less evident because of the greater influence of the frictionally-generated small eddies. The heat flux (Q_H) given by equation 2.12 should correspond to the time-average of the instantaneous flux.

A similar set of observations under stable conditions would show that both w and T have traces similar in form to that of the lower trace in Figure 2.11 (i.e. small fluctuations with no longer-period buoyant waves). The w and T fluctuations would tend to be in antiphase with each other due to the inverted T profile. Using similar reasoning to that for the unstable case it can be seen that both up- and downdrafts will tend to result in a net downward heat flux through the measurement level.

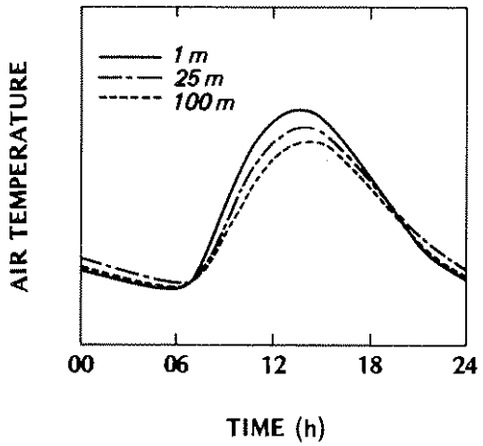

Figure 2.13 Generalized daily cycle of air temperature at three different heights in the atmosphere on a cloudless day.

In neutral conditions the w trace would again only be composed of small forced convection fluctuations, but the T trace would show virtually no variation with time. This is because although eddies are moving through the measurement level they thermodynamically adjust their temperature during ascent or descent so that they are always at the same value as the mean environmental temperature. The net heat flux is therefore zero.

The diurnal surface temperature wave penetrates up into the atmosphere (Figure 2.13) mainly via vertical turbulent transfer (Q_H). The upward migration of this wave is analogous to that in the soil (Figure 2.6) in that there is a time lag for the wave to reach greater distances from the surface, and the wave amplitude decreases (Figure 1.10b). There is however a considerable difference between the rates and distances travelled in the two media. In the soil these are controlled by the value of κ_{Hs} (equations 2.6 and 2.7) but in the atmosphere by K_H. The latter is very much more efficient. This explains why the air temperature wave in Figure 2.13 penetrates to a height of 100 m with only a slight lag and little reduction in amplitude. On an unstable afternoon surface heated air parcels may reach as high as 2 km.

Figure 2.14 shows the temporal development of the vertical temperature structure near the ground during an 'ideal' day. In our discussion we will progress from left to right through the profiles. At night (profile 1) the surface radiation budget is negative due to long-wave emission and so the surface cools to a temperature below that of the air above, producing a ground-based *radiation inversion*. This creates an air temperature gradient

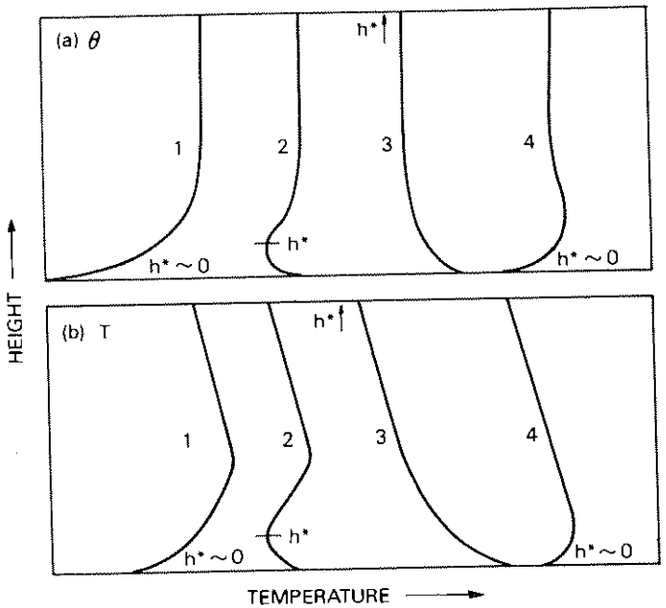

Figure 2.14 Generalized form of the air temperature profile in the lowest 150 m of the atmosphere at different times on a day with fine weather. Profiles: 1 – before sunrise, 2 – soon after sunrise, 3 – midday, 4 – near sunset. The same profiles are plotted in (a) using potential temperature (θ), and (b) using environmental temperature (T) (see p. 53 for an explanation). The depth of the mixed layer (h^*) is also indicated.

directed towards the surface, so that any air motion results in a downward sensible heat flux. The sensible heat flux divergence extends the cooling to affect a depth of about 50–100 m by just before sunrise. The layer is usually strongly stable and there is no mixed layer (h^*) near the surface. This profile is the same as those in Figures 2.2 and 2.4b. Above the inversion a neutral or weakly stable layer exists as a remnant of the previous day's mixed layer.

Soon after sunrise the surface radiation budget becomes positive and the surface temperature rises. This generates an upward sensible heat flux which converges into only the lowest air layer because convective activity is suppressed by the existence of the radiation inversion above. Hence profile 2 in Figure 2.14 is formed, with a shallow mixed layer surmounted by the remnant nocturnal inversion.

Continued turbulent heat convergence into the lowest atmosphere successively erodes the inversion layer until by mid-morning it is eliminated. Thereafter the convectively-driven mixed layer can more readily extend up

through the overlying air. By midday a lapse profile extends throughout a deep unstable layer (profile 3 in Figure 2.14) and the temperature profile near the surface is the same as in Figures 2.2 and 2.4a. Just before sunset (profile 4), the surface radiation budget turns negative and surface cooling re-establishes the radiation inversion in a shallow layer at the ground. This cuts off the mixed layer from its source of heat and it collapses (Figure 2.18a, p. 72).

The preceding very idealized conditions are of course greatly modified by weather conditions, especially cloud cover and wind speed through their impact on radiation and turbulence respectively. In general increases of cloud and wind cause a reduction in the daily range of temperature (lower maxima and higher minima) and reduce extremes of stability (more neutral). Instruments to measure surface, soil and air temperatures, and methods to calculate the turbulent sensible heat flux density, are given in Appendix A2).

(d) Water vapour and latent heat fluxes (E, Q_E) and atmospheric humidity (ρ_v or e)

Prior to a discussion of the transfer of water vapour between the surface and the surface layer, which is so important because of its energetic, hydrologic and biological implications, it is necessary to explain how we will represent the vapour content (humidity) of air. There are many ways to express humidity. To avoid confusion we will restrict concern to two basic, and simply related, measures: vapour pressure and vapour density.

Vapour density (ρ_v) is one of the most basic ways of expressing the vapour content of air. It simply relates to the mass of water vapour molecules in a volume of air and therefore has units of kg m^{-3} (or g m^{-3} to avoid very small numbers). Vapour density is also referred to as 'vapour concentration' or 'absolute humidity'.

The *vapour pressure* (e) is a measure of the partial pressure exerted by water vapour molecules in the air. Typical values of vapour pressure are less than 4 kPa which is very small when compared to the 97 to 103 kPa total atmospheric pressure (P) registered on weather maps.

These two measures are related through the Ideal Gas Law written in the form:

$$e = \rho_v R_v T$$

where R_v is the specific gas constant for water vapour = 461·5 J kg^{-1} K^{-1}. Therefore a simple, approximate conversion is:

$$\rho = 2{\cdot}17 \cdot e/T$$

with ρ_v in g m^{-3}, e in Pa and T in kelvins.

Saturation is an important concept in humidity. Consider a bowl of pure

water introduced into a closed container of dry air. A water-to-air vapour gradient will exist and molecules will diffuse into the air, thereby increasing the vapour density (and vapour pressure). This progressively weakens the gradient and eventually an equilibrium is established where the molecules escaping to the air are balanced by those returning to the liquid. The air is then said to be saturated and the humidity values are the *saturation vapour density* (ρ_v^*) and the *saturation vapour pressure* (e^*). If the temperature of the water is raised the kinetic energy of the molecules is increased, more are able to escape, and the saturation level is greater. For a plane surface of pure water the saturation humidity versus temperature relationship is very well defined. That for e^* is shown in Figure 2.15. Values for both ρ_v^* and e^* for a wide range of temperatures are listed in Appendix A3, p. 394. The figure and Appendix A3 also show that saturation values over an ice surface are slightly lower. The saturation humidity versus temperature relation is a very important one, especially when studying evaporation from water surfaces or condensation of water upon surfaces.

Most of the time the atmosphere is not saturated, i.e. most air samples plotted on Figure 2.15 would lie to the right of the curve, like sample A at a temperature of 15°C with e = 1000 Pa (or $\rho_v \sim 7{\cdot}53$ g m^{-3}). For many purposes it is useful or important to know how far the air is from being saturated. This can be expressed in many ways but we will restrict ourselves to two; they relate to the two ways a sample can become saturated. First, if the temperature were held constant, but more vapour were added, the sample will eventually saturate. The amount of vapour necessary to achieve this is called the *vapour pressure (or density) deficit*, vpd or vdd respectively, i.e.:

$$\text{vpd} = (e^* - e) \tag{2.13a}$$

$$\text{vdd} = (\rho_v^* - \rho_v) \tag{2.13b}$$

For sample A the saturation value is found by extending a vertical line through A to the intersection with the saturation curve where we see (Figure 2.15 and Appendix A3, p. 394) that e^* = 1704 Pa (or ρ_v^* 12·83 g m^{-3}), so that vpd = 704 Pa (vdd ~5·3 g m^{-3}). In a simple way the deficit may be thought of as the 'drying power' of air relative to a saturated surface such as a leaf stomate or a lake; the greater the deficit the greater the vapour gradient to drive evaporation right at the surface where the air and surface have almost the same temperature. On the other hand, it is not a good measure to use to compare humidity at two very different locations because its definition (equation 2.13) includes temperature in the saturated term.

Secondly, if the vapour content remained the same but the sample were cooled by removing heat, it will eventually become saturated. The temperature at which this occurs is called the *dew-point* (or *frost-point* if

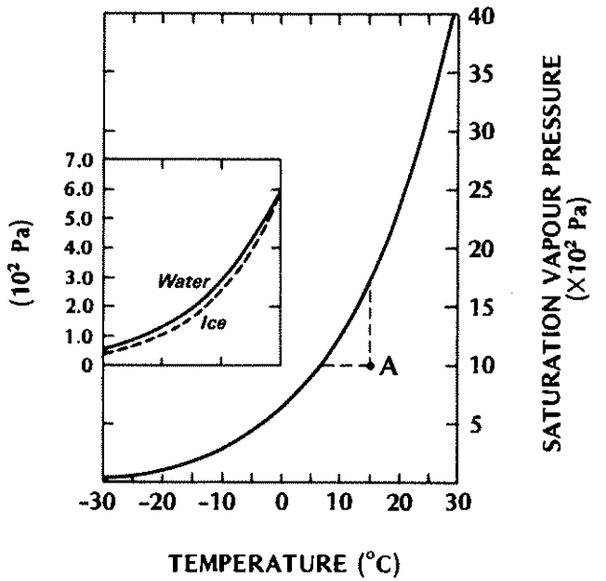

Figure 2.15 Relationship between saturation vapour pressure (e^*) over a plane surface of pure water, and temperature. Inset: Saturation vapour pressure over water and ice at temperatures below 0°C. The corresponding curve for saturation vapour density is very similar.

it is below 0°C). In Figure 2.15 this is ~7°C, found by extrapolating a horizontal line through A to intersect the saturation curve. The dew-point temperature is very useful when considering condensation of fog or dewfall due to cooling.

Evaporation from the surface passes through the laminar boundary layer according to equation 2.4b. In the turbulent surface layer this mass flux is given by:

$$E = -K_V \frac{\partial \bar{\rho}_v}{\partial z} \tag{2.14}$$

where, K_v – eddy diffusivity for water vapour (m^2 s^{-1}). The energy required to vaporize the water is considerable (p. 28) and the accompanying flux of latent heat is given by substituting equation 1.21 in 2.14:

$$Q_E = -L_v K_V \frac{\partial \bar{\rho}_v}{\partial z} \tag{2.15}$$

The evaporation process depends not only upon the availability of water but also upon the availability of energy to enable change of state; the

existence of a vapour concentration gradient; and a turbulent atmosphere to carry the vapour away.

The exchange of moisture between the surface and the atmosphere determines the humidity, just as the sensible heat flux largely governs the temperature in the lowest layers. However, whereas heat is pumped into the air by day and returned to the surface by night, the flux of water is overwhelmingly upward. The evaporative loss is strongest by day, but often continues at a reduced rate throughout the night. Under certain conditions this loss may be halted and water is returned to the surface as *dew*, but in comparison with the daytime mass flow it is almost negligible. The water put into the atmosphere is of course returned by the process of precipitation rather than by turbulence.

By day the profile of vapour concentration lapses with height away from the surface moisture source (Figure 2.16a and b) in the same manner as the temperature profile (Figure 2.2). Vapour is transported upwards by eddy diffusion in a process analogous to that for sensible heat. If the temperature (T) trace in Figure 2.12 were replaced with that for vapour density (ρ_v) then the associated flux would be that of water vapour (E), or with appropriate modification, of latent heat (Q_E).

In the morning hours the evapotranspiration of surface water (dew, soil water, and plant water) into a moderately unstable atmosphere adds moisture (by flux convergence) to the lower layers and the humidity increases quite sharply (Figure 2.16b). By the early afternoon, although E is at a peak the humidity concentration drops slightly. This is the result of convective activity having penetrated to such heights in the boundary layer that the vapour concentration becomes diluted by mixture with descending masses of drier air from above. This feature is best seen at continental or desert stations where regional air masses are dry, and surface heating is strong. (The rural data in Figure 8.17, p. 295, are an example from a continental station.) In the late afternoon surface cooling is strong and the lowest layers become stable. Thus the ability to transport vapour to higher layers is less than the rate at which it continues to be added from the surface. Moisture converges into the lowest layers and a second humidity maximum is observed (Figure 2.16b). Thereafter evapotranspiration declines into the night period. Under certain conditions (see below) the vapour profile may become inverted near the surface (Figure 2.16a) so that vapour is transferred downwards as dewfall. This depletes the moisture in the lowest layers and humidities decrease (Figure 2.16b), until after sunrise when the cycle re-commences. Instruments to measure humidity, and methods to calculate evapotranspiration, are presented in Appendix A2.

Radiative cooling at night may cause the surface temperature to fall below that of the contacting moist air. The ensuing condensation on the surface gives rise to an inverted lapse rate so that turbulence leads to a downward flux and further deposition. The process of *dewfall* is therefore

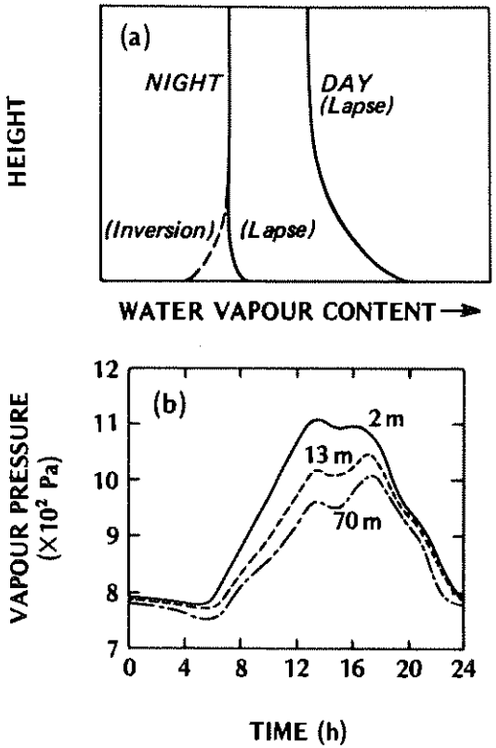

Figure 2.16 (a) Idealized mean profiles of water vapour concentration near the ground's surface, and (b) the diurnal variation of vapour pressure at 3 heights at Quickborn, Germany on cloudless days in May (after Deacon, 1969, using data of Frankenberger).

a quasi-turbulent phenomenon requiring wind speeds to lie within a critical range. If the air is calm the loss of moisture to the ground cannot be replenished from more humid layers above and dewfall ceases. On the other hand if winds are too vigorous the surface radiative cooling (L^*) is offset by turbulent warming (Q_H), and the vapour inversion is destroyed. The critical wind speed depends upon the roughness of the surface. For a short grass surface a minimum wind speed of 0·5 m s^{-1} at 2 m is required (Monteith, 1957). If the dew freezes, or if the vapour originally sublimates rather than condenses upon the surface, the deposit is called *hoar frost*.

Radiation or ground fog is another humidity-related phenomenon observed on cloudless nights with light winds. (Figure 2.17). It commonly forms over moist or marshy ground on such nights, and as with dewfall it

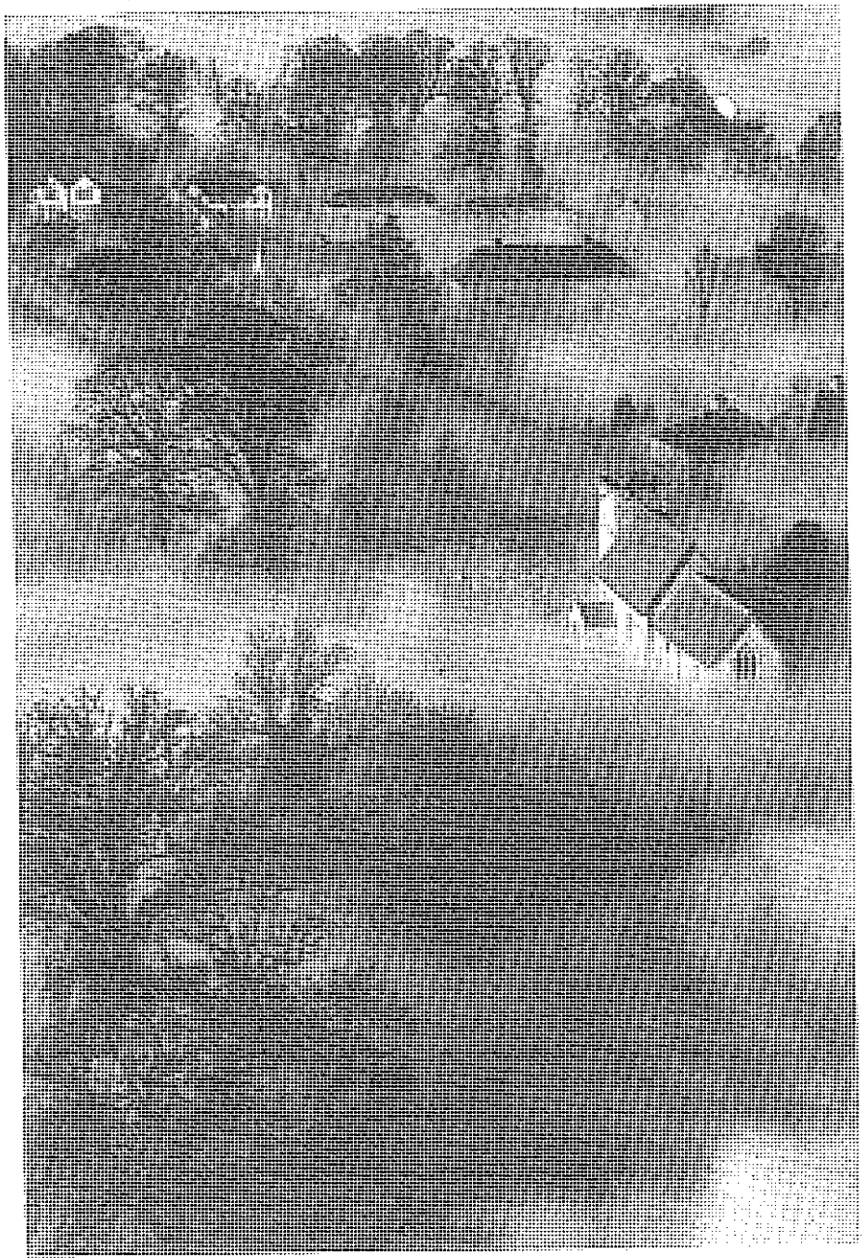

Figure 2.17 Radiation fog over Little Wymondley. Note the fog is only about 5 m deep and thins around buildings. This may be due to their warmth or because radiative cooling is less where the sky is partially obscured (see p. 133).

is the result of a fine balance between radiative cooling and turbulent warming of an air layer (volume) near the surface. The process is particularly aided if the air is humid and close to saturation in the evening, and if the air aloft is relatively dry. Under these conditions the moist surface air layer has a strongly negative long-wave radiation budget because it radiates more energy than it receives from the colder surface beneath. Similarly it emits more than it receives in its exchange with the air above because its vapour content gives it a greater emissivity. The layer therefore cools by long-wave radiative flux divergence ($-\Delta L^*$). On cooling to its dew-point it becomes saturated and fog droplets develop. The fog formation is aided by light winds which enhance the loss of sensible heat from the layer to the surface (Q_H), but beyond a certain limit increased winds thwart fog formation by increasing turbulent mixing which weakens the inversion strength and dilutes the moisture concentration. (See Figure 2.7.)

Once a fog bank has formed the active radiating surface becomes the fog top and not the surface of the ground because the water droplets are almost full radiators for long-wave radiation (p. 15). They therefore absorb and emit very efficiently at these wavelengths and hence $L\uparrow$ from the fog top continues to cool it and helps the fog to become progressively thicker.

Radiation fogs usually linger for a few hours after sunrise, and can last all day aided by the high albedo of the fog top. Fog dissipation does not usually result from solar heating of the droplets, but by convection generated at the surface or by increased wind speeds. In both cases the mixing of the fog with drier air is the cause of its disappearance.

Other types of fog, formed by very different processes are explained on p. 165.

(e) Further remarks on convective exchange

Convection is the principal means of transporting the daytime energy surplus of the surface away from the interface. The relative importance of sensible versus latent heat is mainly governed by the availability of water for evaporation, although the relative strengths of the atmospheric heat and water vapour sinks are also important. For example if an abnormally cold and moist air mass settles over a region it would strengthen the daytime surface-air temperature gradient, and diminish the vapour gradient. Inspection of equations 2.12 and 2.15 shows that this would favour Q_H rather than Q_E.

The energy partitioning between Q_H and Q_E has direct relevance to boundary layer climates. The ratio of these two fluxes is called *Bowen's ratio* (β) so that:

$$\beta = Q_H/Q_E \qquad (2.16)$$

Thus if β is greater than unity, Q_H is larger than Q_E as a channel for dissipating heat. This may be found over surfaces where water is to some extent limited. Since a majority of the heat being convected into the atmosphere is in the sensible form the climate is likely to be relatively warm. On the other hand if β is less than unity, Q_E is larger than Q_H, and the heat input to the atmosphere is mainly in the latent form. This will not directly contribute to warming of the lower atmosphere, but may increase its humidity. Therefore the climate is likely to be relatively cool and moist. Negative β values merely indicate that the two fluxes have different signs. This is common at night when the sensible heat flux is downwards (negative), but evaporation continues so that Q_E is away from the surface (positive). Typical average values of β are 0·1 for tropical oceans; 0·1 to 0·3 for tropical wet jungles; 0·4 to 0·8 for temperate forests and grassland; 2·0 to 6·0 for semi-arid areas; and greater than 10·0 for deserts.

Although we have concentrated on the turbulent transport of heat, water vapour and momentum, other substances are also convected to and from the atmosphere. For example the flux of carbon dioxide may be represented by the flux-gradient equation:

$$F_C = -K_C \frac{\partial \bar{\rho}_c}{\partial z} \tag{2.17}$$

where F_C – flux density of CO_2 (kg m^{-2} s^{-1}), K_C – eddy diffusivity for CO_2 (m^2 s^{-1}), and ρ_c – CO_2 concentration (kg m^{-3}). Similar relationships could be constructed for carbon monoxide, ozone, pollen, spores, dust, etc. The major requirements are that the substances should be inert (so that they do not decay quickly), and lightweight (so that gravitational settling does not deplete the concentration).

The convective exchange of entities between a surface and the atmosphere can usefully be viewed as a simple analogue of the flow of current (electrons) in an electrical circuit due to the electrical potential across its ends and the resistance to this flow provided by the wire. The relationship is given by Ohm's Law:

$$\text{Current (amps)} = \frac{\text{Potential difference (volts)}}{\text{Wire resistance (ohms)}}$$

and the analogue for the flux of other entities may be written:

$$\text{Flux rate} = \frac{\text{Concentration difference}}{\text{Resistance to flow}}$$

so that substituting the appropriate climatological terms we have:

Sensible heat	$Q_H = (C_a \Delta \overline{T})/r$	(2.18a)
Water vapour	$E = \Delta \bar{\rho}_v / r$	(2.18b)

Momentum	$\tau = -(\rho \Delta \overline{u})/r$	(2.18c)
Carbon dioxide	$F_C = \Delta \bar{\rho}_c / r$	(2.18d)

where r represents the appropriate system *resistance* (s m^{-1}). For some purposes it may be useful to use the reciprocal of resistance (r^{-1}) which is called the *conductance*. It can be shown (Munn, 1970) that the value of r depends on the thickness of the layer concerned and its ability to transport the entity. Therefore r acts as the inverse of the molecular and eddy diffusion coefficients (the κ's and K's) in the standard flux-gradient equations introduced earlier in this chapter. The diffusion coefficients represent the facilitating role of the system in transferring quantities, conversely the resistance represents the degree of hindrance to flow.

This *electrical analogy* is helpful in simplifying some calculations and it helps aid discussion between atmospheric scientists, physiologists and engineers because they are all familiar with this approach. It is commonly used in relation to leaves and vegetation communities, animals (including humans), buildings and air pollution deposition. The diffusion of entities can be represented in the same manner as an electrical circuit diagram and the same rules apply. Resistances can be added together in series (end to end) $r = r_1 + r_2$, or in parallel (side by side) $r = 1/r_1 + 1/r_2$. The former can be used to characterize transport through a number of layers, e.g. the flow of heat from an internally heated house through the wall layers and the outside wall laminar sub-layer out to the atmosphere. The latter could be used to sum the heat loss from various pathways out of the house, e.g. through the windows, the roof and the basement as well as the walls. The electrical analogy can even be extended to include capacitors in the circuitry to play the role of heat or mass stores.

The K's and the r's discussed in this chapter are not necessarily the same for different entities. This is a matter of great debate in micrometeorology. Nevertheless, it is reasonably accepted to say that all other things being equal, the transfer coefficients for heat and mass are reasonably similar but the case for momentum is different (see also pp. 378 and 382).

4 OUTER LAYER CLIMATES

The planetary boundary layer is continually evolving in response to the daily heating/cooling cycle and to changing synoptic conditions. The temporal dynamics of the boundary layer under 'ideal' weather conditions are illustrated in Figure 2.18a.

As noted in relation to Figure 2.14 the mixed layer, of depth h^*, starts to rise when the surface sensible heat flux density (Q_H) becomes positive. After 'pinching out' and eliminating the previous night's inversion it rapidly deepens to its maximum value in mid-afternoon and the complete layer is convectively unstable. The mixing equalizes temperature, wind speed,

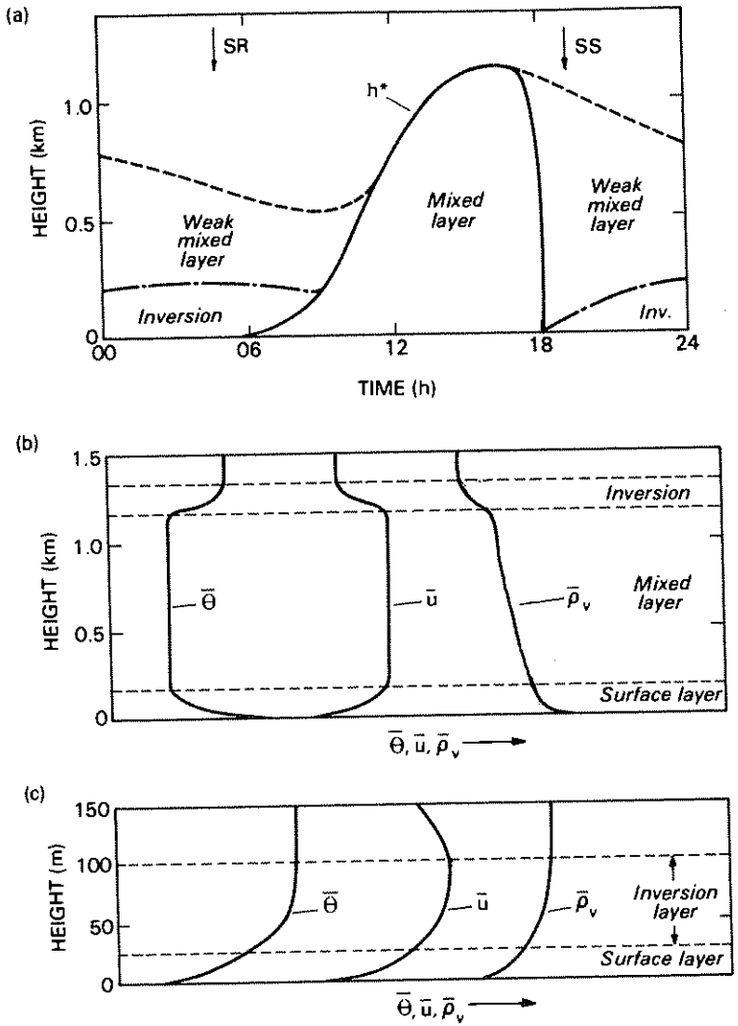

Figure 2.18 (a) Daily variation of the boundary layer on an 'ideal' day. (b) Idealized mean profiles of potential temperature ($\bar{\theta}$), wind speed ($\bar{u}$) and vapour density ($\bar{\rho}_v$) for the daytime convective boundary layer. (c) Same as (b) for nocturnal stable layer. The arrows in (a) indicate times of sunrise and sunset.

humidity and other properties throughout the layer (see Figure 2.18b). Sharp changes in these profiles occur at the top of the mixed layer where a capping inversion often halts the upward transport of surface effects.

The principal agents of transport and mixing in the mixed layer are

thermals. These are rising masses of warm air. The sequence in Figure 2.19a illustrates the temporal development of a thermal when there is little or no horizontal wind. It starts as an area of especially warm air at the surface. Favoured sites which act as sources for thermals are relatively dry areas (bare soil, rock, asphalt or sands) and Sun-facing slopes. The hot air forms a flattened bubble until the instability becomes sufficient to cause it to start to rise. Whereupon it contracts, becomes more spherical and lifts off. The thermal grows in size as it rises due to the entrainment of surrounding air. The action is similar to that of a smoke-ring as the thermal seems to be continually trying to turn itself inside out. The size of the thermal depends on the dimensions of the source area, and the rate of rise upon the degree of instability. Initially the velocity increases but at greater heights it slows down due to the mixing with cooler air and increasing drag due to its size. The thermal ceases to rise because (i) it has lost buoyancy by mixing, (ii) its moisture condenses into cloud and the extra turbulence due to the release of latent heat causes even greater mixing or because (iii) it reaches an inversion.

If surface winds are moderate a surface hump can act as a trigger for thermals in the manner shown in Figure 2.19b. This may spawn a series of thermals which drift downstream and may become visible as a line of cumulus clouds. Hills and islands often play this role. If the windward slope is oriented favourably with respect to direct-beam solar radiation its surface heat may be the source of semi-continuous columns of thermals.

It is quite typical to have an array of thermal sources across the landscape providing preferred 'columns' of uplift extending through the depth of the mixed layer and perhaps identified by cumulus clouds. The intervening, and larger, areas are occupied by subsiding air. Together they form Bénard convection cells as shown in Figure 2.4a (p. 42).

If in the morning and evening, when convection is less vigorous, the surface wind speed is in excess of about 6 m s^{-1} the cells may become organized into roll structures aligned parallel to the wind. If cloud forms at the top of the uplift zone between two adjacent rolls the cumulus clouds form into lines known as *cloud streets* (Figure 2.19c). There is also the possibility that the cloud pattern reinforces the roll structure by creating alternating strips of shade and sunlight on the ground.

The formation of a layer of cumulus clouds just above the condensation level can raise the moisture concentration gradually to the point where the whole layer becomes saturated and stratus (layer) cloud forms. Similarly, if moist thermals are stopped rising by an inversion, stratus cloud or a haze layer can form at the top of the mixed layer. This may significantly affect the transmission of solar radiation to the ground and dampen convective activity.

Whether cumulus clouds remain relatively small or undergo significant vertical development (possibly leading to precipitation or a severe storm) is

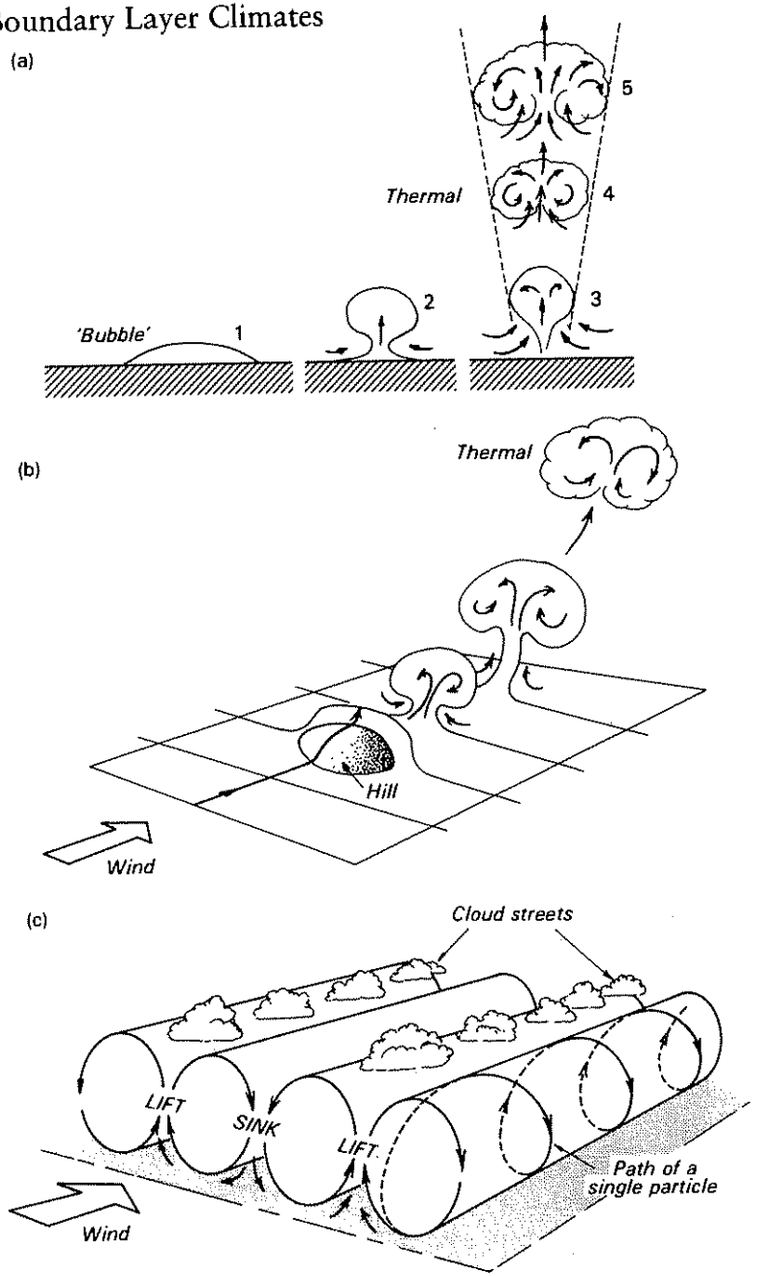

Figure 2.19 Convective structures associated with instability. (a) Stages in the temporal development of a thermal. (b) Initiation of a thermal by a hill. (c) Formation of clond streets (based on Scorer, 1978).

largely dependent upon the strength of any capping inversion and the stability of the air *above* the planetary boundary layer.

In the evening when radiative cooling begins, and the surface sensible heat flux density becomes negative, the surface-based radiation inversion begins to grow in depth and cuts off the mixed layer from its source of heat and buoyancy (Figure 2.18a). Turbulence in the mixed layer decays, only roughness-generated turbulence persists near the surface, and the surface vertical profiles of temperature and humidity reverse sign because the surface is now a sink for heat and, to a lesser extent, water vapour (Figure 2.18c). The wind profile may exhibit a wind maximum located near the top of the inversion. This is known as the *low-level nocturnal jet.* It arises because the stability of the surface inversion decouples the air above it from the frictional influence of the surface. The depth of the inversion and the turbulent layer are not necessarily synonymous. With very weak winds and clear skies, increasing stability chokes off turbulence in the upper portion of the inversion and the mechanical mixing is restricted to an even thinner layer.

The degree of coupling between the surface and the rest of the boundary layer varies through the day and is responsible for the commonly observed diurnal variation of wind speed (Figure 3.1, p. 80). During the daytime vertical coupling is excellent and the momentum of faster-moving upper air is easily transported downward and mixed into the surface layer. This contributes to high wind speeds. At night poor coupling prevents this process, so wind speeds slacken. The drop in wind speed around sunset is often very noticeable.

Air motion is of course a vector quantity possessing both magnitude (speed) and direction. At the top of the planetary boundary layer the effects of surface friction are absent so the wind is dictated by the strength and orientation of the horizontal pressure gradient force. The force, and therefore the speed, varies inversely with the isobar spacing on the weather map. This is the *gradient wind speed* at the height z_g in Figure 2.10a. Because the Earth rotates, the gradient wind direction is not, as we might anticipate, from high to low pressure but almost parallel to the isobars. The Coriolis force causes the deflection to the right of the intended path in the Northern, and to the left in the Southern, Hemisphere. This is embodied in Buys Ballot's Law: if you stand with your back to the wind in the Northern Hemisphere you will have low pressure on your left-hand side.

As the surface is approached, friction reduces the wind speed (Figure 2.10a) and correspondingly reduces the Coriolis force, which depends on the air density, latitude and wind speed. This alters the balance of forces, and the wind direction changes so that it cuts the isobars at an increasingly large angle the nearer it is to the surface. In the Northern Hemisphere the direction changes in an anti-clockwise manner, referred to as *backing* (in

the Southern Hemisphere it would turn clockwise, called *veering*). Since surface roughness differences produce changes of wind speed at the same elevation (Figure 2.10a) it follows that the backing angle is also altered. Over typical land surfaces the surface (10 metre level) wind is backed by about 30 to 40 degrees, from the gradient wind direction. Over water bodies it is closer to 15 degrees. Therefore, as air flows from one surface to another of different roughness both the speed and direction are changed (see Chapter 5). Further, since stability affects the vertical transport of momentum its variability can also affect the wind direction.

It should be appreciated that the evening collapse of the mixed layer does not mean that the lid physically pushes down. Pollutants that are diffused throughout the daytime mixed layer do not get squeezed down near the surface. They remain suspended in the weakly turbulent vestigial mixed layer until transported out horizontally, or removed by settling or precipitation, or transformed chemically.

In keeping with the rest of our discussions to this point the preceding only relates to horizontal, spatially-uniform terrain in fine weather. In Chapter 5 we will relax the terrain constraint. The effects of increased cloud and wind tend to mute the slope of vertical profiles and the day-to-night variations shown here. Naturally short-term changes in synoptic conditions will disrupt the temporal patterns.

Part II

Natural atmospheric environments

In this part of the book we consider the boundary layer climates associated with a wide range of natural surfaces and systems. The text is organized in a progression from relatively simple surfaces to more complex systems. Thus we start with environments where the surface is relatively flat, uniform in character and extensive (e.g. bare soil and sandy desert). Then we consider systems where this straightforward situation is complicated by the fact that the surface is semi-transparent to radiation (e.g. snow and ice), and the system is able to transmit heat by internal convection (e.g. water). Next we introduce a layer of vegetation between the soil and the atmosphere, and then the complicating effects of sloping and hilly terrain, and the advective interaction between the climates of adjacent contrasting surfaces. Finally in this part we consider the climates of animals. These represent some of the most complex climatic systems because they are able to move from one environment to another, and they carry with them their own internal energy supply (metabolic heat).